

A new repository of electrical resistivity tomography and ground penetrating radar data from summer 2022 near Ny-Ålesund, Svalbard

Francesca Pace¹, Andrea Vergnano², Alberto Godio¹, Gerardo Romano³, Luigi Capozzoli⁴, Ilaria Baneschi⁵, Marco Doveri⁶,
5 Alessandro Santilano⁷

¹ Department of Environment, Land and Infrastructure Engineering (DIATI), Politecnico di Torino, Turin, 10129, Italy.

² Department of Earth Sciences (DST), Università degli Studi di Torino, Turin, 10125, Italy.

³ Dipartimento di Scienze della Terra e Geoambientali, Università degli Studi di Bari Aldo Moro, Bari, 70125, Italy.

⁴ Institute of Methodologies for Environmental Analysis, National Research Council (CNR), Tito, 85050, Italy

10 ⁵Geosciences and Earth Resources (IGG) - National Research Council of Italy (CNR), Pisa, 56124, Italy

⁶ Dipartimento di Scienze della Terra, Pisa University, Pisa, 56126, Italy.

⁷Geosciences and Earth Resources (IGG) - National Research Council of Italy (CNR), Messina, 98166, Italy

15 *Correspondence to:* Francesca Pace (francesca.pace@polito.it)

Abstract.

We present the geophysical data set acquired in the summer of 2022 close to Ny-Ålesund (Western Svalbard, Brøggerhalvøya peninsula - Norway) as part of the project ICEtoFLUX. The aim of the investigation is to characterize the role of groundwater flow in correspondence of the active layer as well as through and/or below the permafrost. The data set
20 is composed of Electrical Resistivity Tomography (ERT) and Ground Penetrating Radar (GPR) surveys, which are well-known geophysical techniques for the characterization of glacial and hydrological processes and features. 18 ERT profiles and 10 GPR lines were acquired, for a total surveyed length of 9.3 km. The data have been organized in a consistent repository that includes both raw and processed (filtered) data. Some representative examples of 2D models of the subsurface are provided, that is, 2D sections of electrical resistivity (from ERT) and 2D radargrams (from GPR). The
25 resistivity models revealed deep resistive structures, probably related to the heterogeneous permafrost, which are often interrupted by electrically conductive regions, that may relate to aquifers and/or faults. The interpretation of these data can support the identification of the active layer, the occurrence of spatial variation of soil conditions at depth, and the presence of groundwater flow through the permafrost. To a large extent, the data set can provide new insight into the hydrological dynamics and polar and climate change studies on the Ny-Ålesund area. The data set is of major relevance because there is
30 little geophysical data published about the Ny-Ålesund area. Moreover, these geophysical data can foster multidisciplinary scientific collaborations in the fields of hydrology, glaciology, climate, geology, geomorphology, etc. The geophysical data are provided in a free repository and can be accessed at the repository under data doi (Pace et al., 2023, <https://zenodo.org/doi/10.5281/zenodo.10260056>).

1 Introduction

35 The Earth's interior and its physical properties are imaged by quantitative methods. Geophysical measurements on the Earth's surface can reveal how the subsurface physical properties vary in space, and possibly in time (Telford et al., 1990). The Svalbard Archipelago (High Arctic Norway, see Fig. 1a) is believed to be a representative typical Arctic critical environment (Dallmann, 2015). The location of the Svalbard Archipelago is ideal for observing the Arctic environment in general, from the perspectives of glaciology, geology, biodiversity, and impact of climate change (Gevers et al., 2023).

40 Climate change heavily affects the Arctic hydrologic dynamics, generating significant environmental modifications and potentially leading to the climatic feedback and warming amplification (Wadhams, 2017). Ny-Ålesund is the northernmost settlement of the world (79° North), located in western Spitsbergen in the Svalbard Archipelago (see Fig. 1b). It serves as a scientific hub for the international research community and its logistical support (Paglia, 2020). Ny-Ålesund represents an outstanding natural lab for any topics of scientific research in the Arctic, being

45 situated in the Kongsfjorden Fjord, where glaciers, rivers, coast, sea, atmosphere, animals, plants and their interaction can be monitored (Gevers et al., 2023; Pedersen et al., 2022). From a geophysical point of view, the Svalbard Archipelago is interesting because of the presence of permafrost with seasonal active layer, springs, aquifers, sea water and old coal mines. Spatial heterogeneity in geophysical properties is expected due to the local lithology and structural framework as well as the geomorphologic features linked to the past movement of the glaciers (Orvin, 1934; Dallmann, 2015).

50 Ny-Ålesund is also an ideal place for hydrogeological studies, because 3 km away from the settlement there is the Bayelva River catchment, where the entire water cycle from the glaciers to the sea can be studied within an area of a few squared kilometers (see Fig. 1c). In formerly glacierized watersheds, hydrologic processes are evolving, with new storage mechanisms and distribution of water resources, such as more persistent rivers and developed groundwater systems. Over the past years, investigations on the Arctic freshwater increased but wide knowledge about processes that govern water flow

55 dynamics in High Arctic basins is still quite limited (Svendsen et al., 2002). Applied geophysics can be of great help to unravel the complexity of the water cycle and to improve knowledge about groundwater flow by means of non-destructive measurements from the surface (Hauck and Kneisel, 2008). Geophysical techniques, such as Electrical Resistivity Tomography (ERT) Ground Penetrating Radar (GPR), passive and active seismic methods (Kula et al., 2018), and electromagnetic induction (EMI) methods (Kasprzak, 2020; Hill, 2020), have been used to

60 survey the Arctic areas all around the world, for example to detect the heterogeneity in the permafrost, to monitor glacial and periglacial processes or to understand the role of ice in the hydrology (Hauck and Kneisel, 2008; Rossi et al., 2022). EMI methods have been adopted in the Svalbard Archipelago to characterize the geology (Beka et al., 2015, 2017b), possible geothermal applications (Beka et al., 2016) and CO₂ storage (Beka et al., 2017a).

This paper focuses on the ERT and the GPR methods for the following reasons. The ERT method has been successfully

65 adopted in the Arctic environment because of its effectiveness in imaging the variation in the electrical resistivity values of aquifers, permafrost, and active layer, both at shallow and higher depth, depending on the chosen acquisition settings. The

electrical resistivity values are typically high for the permafrost and low for the water-saturated soil, so that they can be easily distinguished. The GPR method is largely adopted for glaciological studies because the radar signal travels easily and with little attenuation in pure ice, reaching hundreds of meters of depth in ideal conditions. Moreover, given that the traveling time and impedance of the GPR signal are based on the dielectric permittivity of the medium, the GPR method can clearly distinguish frozen from non-frozen conditions, because ice and water have different values of dielectric permittivity. Several goals have been achieved by investigating the permafrost by means of GPR or ERT methods (or their combination), to monitor its temporal variations (Westermann et al., 2010), its physical properties (Schwamborn et al., 2005), the properties of the patterned ground typical of permafrost areas (Park et al., 2023), its water content coupled with Time Domain Reflectometry (Lee et al., 2018), its impacts on quarry activities (Koster and Kruse, 2016), and landslide phenomena (Kuschel et al., 2019).

The surroundings of Ny-Ålesund have been previously investigated by means of ERT surveys for glacier and landslide monitoring (Kuschel et al., 2019; Park et al., 2023) and GPR surveys for glaciological studies (Westermann et al., 2010; Schwamborn et al., 2005; Koster and Kruse, 2016). The Research in Svalbard Portal provides the list of the past and present projects carried out around Ny-Ålesund and adopting geophysical techniques. A non-exhaustive list is composed of the projects PRISM, SEISMOGLAC and CalvingSEIS, GRAVITE, among the others. Other non-geophysical studies focusing on the surroundings of Ny-Ålesund include borehole investigations, geotechnical surveys, numerical modeling and other complementary measurements of the soil or groundwater. The Bayelva River catchment (Fig. 1c) has been largely investigated from a glaciological standpoint (Boike et al., 2018), but there are sporadic studies on its freshwater (Doveri et al., 2019; Repp, 1988; Haldorsen and Heim, 1999; Killingtveit et al., 2003).

However, even though numerous studies about Ny-Ålesund adopted ERT or GPR techniques, most of them did not focus on the characterization of the permafrost, that was mainly investigated by boreholes. In addition, no research has been found that provided spatially extensive information about the permafrost distribution all over the Ny-Ålesund area, at both scales of the active layer and deep aquifers.

The ICEtoFLUX (I2F) project has been funded by the Italian Plan for Research in the Arctic and stands for HydrologIcal changes in ArctiC Environments and water-driven biogeochemical FLUXes (<https://www.icetoflux.eu/>). I2F focuses on the hydrologic dynamics and related effects in the Bayelva River catchment, from its glacial and periglacial systems down to the Kongsfjorden Fjord sector affected by the river. Experimental activities on hydrology, geo- and environmental chemistry, microbiology and geophysics, and numerical modelling, all concerning water cycle components, were planned and carried out to quantify hydrologic processes and related biotic-abiotic transports. Four piezometers were drilled and monitored in the frame of the I2F project to be used as benchmark for the geophysical study.

We carried out an integrated geophysical survey in the proglacial zone of the glaciers Vestre and Austre Brøggerbreen close to the Ny-Ålesund settlement (Fig. 1c). The geophysical techniques adopted were the ERT and the GPR methods, due to their well-established advantages in the Arctic environment, and the Magnetotelluric (MT) method for its high investigation depth (from hundreds of meters to tens of kilometers). The objective of the geophysical survey relies on the study of the

presence and role of groundwater flow in correspondence of the active layer as well as through and/or below the permafrost. A specific target is represented by the possible groundwater flow at the basis or through the permafrost and the circulation at a depth where the ground is supposed to be permanently frozen. The geophysical survey is also aimed to support the multidisciplinary study about the interactions between superficial water, groundwater circulating in the active layer and deep
105 aquifer.

This paper presents the collection of geophysical data acquired in summer 2022 as part of the I2F project. The objective of this paper is to make available the data set to the scientific community and hence foster advances, interpretations and collaborations with and among the stakeholders. The data here presented are intended to provide a major contribution to research because there have been few studies that have published geophysical data from the Ny-Ålesund area so far.

110 This paper begins by introducing the study area where the geophysical data were acquired. Then, it describes the geophysical survey, the acquisition configurations, and the challenges encountered in the remote Arctic environment. Another section is concerned with the raw data set and the processed data after quality control. Some representative geophysical models are presented. Then, the organization of the repository and of the data files are carefully described. Finally, some hints for discussion, interpretation and avenues for future research conclude the paper.

115 **2 The study area**

The study area is located on the South-Western coast of the Kongsfjorden Fjord at 78°55' northern latitude in correspondence of Ny-Ålesund. The Ny-Ålesund settlement is a polar scientific outpost on the Brøggerhalvøya peninsula that is surrounded by tundra and glaciers (Brøggerbreen and Lovénbreen) on the one side and faces the Kongsfjorden Fjord on the other side. Mt. Zeppelin stands out in the area (see Fig. 1c).

120 The history of this Arctic region is necessarily tied together with the geoscientific exploration by pioneers driven by the thirst for knowledge or by the urge to run the (black) gold rush, being this land rich in coal deposits (Dallmann, 2015). The geology of this has been accurately investigated since the beginning of the 20th century with a particular focus on the coal ore deposits that were exploited until 1962 (Hoel, 1925; Orvin, 1934).

The Svalbard Archipelago is located in the north-western corner of the Eurasian plate, as shown in Fig. 1a (Horota et al.,
125 2023). The outcropping rocks in the Archipelago represent a natural geological archive of the Earth' evolution since its early history, from Archean to recent times. Major tectonic events affected the bedrock of the Svalbard Islands including the Caledonian orogeny, which resulted in the deformation of the Pre-Devonian metamorphic and sedimentary basement. Svalbard's sedimentary succession from Devonian to Paleogene is nearly complete and comprises a wide range of lithologies (conglomerates, sandstones, shales, carbonates, and evaporites). The main rock types are dated from Carboniferous and
130 Permian (limestones and dolomites) to Tertiary sandstones (Fig. 2). Widespread moraines deposits occur in the study area.

In the 20th century, the area hosted the northernmost productive coal field in the world. The coal seams are of Tertiary age, Paleocene or Eocene (Hoel, 1925). The strata briefly consist of sandstones, with subordinate layers of conglomerates, shales,

and coal. The coal seams are concentrated in the lower and upper parts of the Triassic sedimentary sequence (Orvin, 1934). In the lower coal horizon, the most important seams are (from down to top) the Ester, Sofie and Advokat seams. The Agnes-
135 Otelie, Josefine, and Ragnhild seams are on the upper horizon.

The mining exploration period (the first half of 20th century) left a heritage of information about the subsurface of Ny-
Ålesund. Several pits and boreholes were drilled into the frozen soil, to reach the coal seams. The pits were deep from 5 to
20 m, while the boreholes were deep up to 100 m. Relative information, stratigraphy and geological sections, mainly
reporting shales, sandstones, and coal, are accurately described in the appendix plates in Orvin (1934). The boreholes
140 pointed out widespread permafrost conditions but were not intended to carefully assess the permafrost extension and spatial
variability, that are hence not possible to be inferred.

Recent studies on the temporal variability of the permafrost have been performed by means of pits and borehole temperature
monitoring. A comprehensive review of the permafrost monitoring activities near Ny-Ålesund can be found in the SESS
report 2018 (Orr et al., 2019). An extensive 20-year borehole data set near the Bayelva river has been published by Boike et
145 al. (2018) and highlights the recent climate variability in Ny-Ålesund.

Near the old mine area, southeast of Ny-Ålesund, between the fjord and the mountain of the Vestre Lovénbreen glacier (Fig.
1c), recent changes in a complex sub-permafrost hydrological network have been studied (Haldorsen et al., 1996). During
the mining period the Tvillingvatnet Lake, in the west side of the mining area, was reported to receive influx water from a
sub-permafrost aquifer. During winter, the lake was not frozen, and the miners discovered nearby a confined aquifer. The
150 sub-permafrost aquifer was fed by glacier waters, probably by the nearby Austre Brøggerbreen, which extended closer to the
lake than today (see Fig. 1c). Nowadays, the Tvillingvatnet Lake freezes during winter, thus suggesting that the sub-
permafrost influx has apparently stopped or greatly reduced. The chemical analyses on the water of the lake showed that it
now probably comes from a supra-permafrost aquifer located in the hillside of the Vestre Lovénbreen mountain (Haldorsen
et al., 2002). A similar fate happened to the Ester Spring, located in the mine area (see Fig. 1c). This spring was reported
155 since the mining period (around 1930) and was characterized by a continuous water flux of multiple liters per second during
winter and constant chemical properties during the year. The spring water was supposed to come from the Vestre
Lovénbreen glacier, to infiltrate into a moulin and then to be heated underground by the geothermal heat. This made it
possible to warm the permafrost and to generate the Ester Spring (Booij et al., 1998; Van der Ploeg, 2002). This flux has
decreased across the last decades and then stopped in 2007. According to the literature, the recent changes observed in the
160 Ester Spring are linked to the global warming effects on the Vestre Lovénbreen glacier (Haldorsen et al., 2011, 2010;
Haldorsen and Heim, 1999). Due to the warming temperatures and thinning of the glacier, it has lost part of its insulation
effect against the cold winter (Pälli et al., 2003). Therefore, the geothermal heat flux is no more able to keep the glacier base
at the pressure-temperature melting point, and the water and heat transfer from the moulin to the Ester Spring could have
stopped (Putkonen, 1998). Supporting this hypothesis, a water flux larger than the past is observed melting at the tongue of
165 the glacier through superficial streams, while in the past the melting at the tongue was minimal.

170 All the above-mentioned studies, while being particularly delved into the specific aspects of the permafrost processes, rely on a few deep boreholes or focuses on specific areas in the surroundings of Ny-Ålesund. Therefore, at this stage it is not possible to depict a comprehensive overview of the spatial variability of the permafrost in the study area, especially at significant depth. In this context, the proposed shallow and deep geophysical investigations (ERT and GPR), that ensure different resolution scales, can fill the gap of knowledge regarding the spatial variability of the permafrost, potentially uncovering features that have not been discovered so far.

175 The geophysical survey of the I2F project was conceived in parallel with hydrogeological investigations. The four piezometers (P1, P2, P3, P4) drilled as part of the I2F project (see the “Piezometer Area” in Fig. 1c) were placed in a dominantly mineral soil in order to continuously monitor the water level, temperature and electrical conductivity of water, to measure periodically the depth of frozen ground and to sample water for chemical and isotopic analyses. High density polyethylene pipes (with a diameter of 63 cm and a length of 3 m) were inserted in predrilled holes down to 200 cm into the soil. Each tube was screened by 3 mm slits in the lower 200 cm to allow water to enter the tube. Once piezometers were installed, caps were placed on top, again preventing outside material from entering the tube. The gravel (2-5 cm of diameter), collected locally to avoid external effects on the chemical features of the water, was placed between the tube and the soil to fill the space around the tube and creating a pre-filter respect to the screened part. The piezometer metadata are available from the Italian Arctic Data Center (IADC) webpage (<https://metadata.iadc.cnr.it/geonetwork/srv/api/records/5e0ba64e-71a7-4949-8752-9fb57b38b4fa>). Moreover, the I2F webpage shows the location and coordinates of piezometers, the network of sampling stations (snow pits, glacial and proglacial drainages, bulk snow) and geophysical surveys (<https://www.icetoflux.eu/data/>). This page will provide the piezometer data from continuous monitoring (including chemical and isotopic water analyses) as soon as the hydrological modeling is completed by the project partners. Some of the piezometer data measured during the geophysical surveys, such as depth of frozen ground, water level and water electrical conductivity and temperature, were used for preliminary interpretation of the geophysical results of this work. Meteorological and climatic data (air temperature and precipitation) can be downloaded from the Ny-Ålesund weather station (SN99910, <https://seklima.met.no>).

190

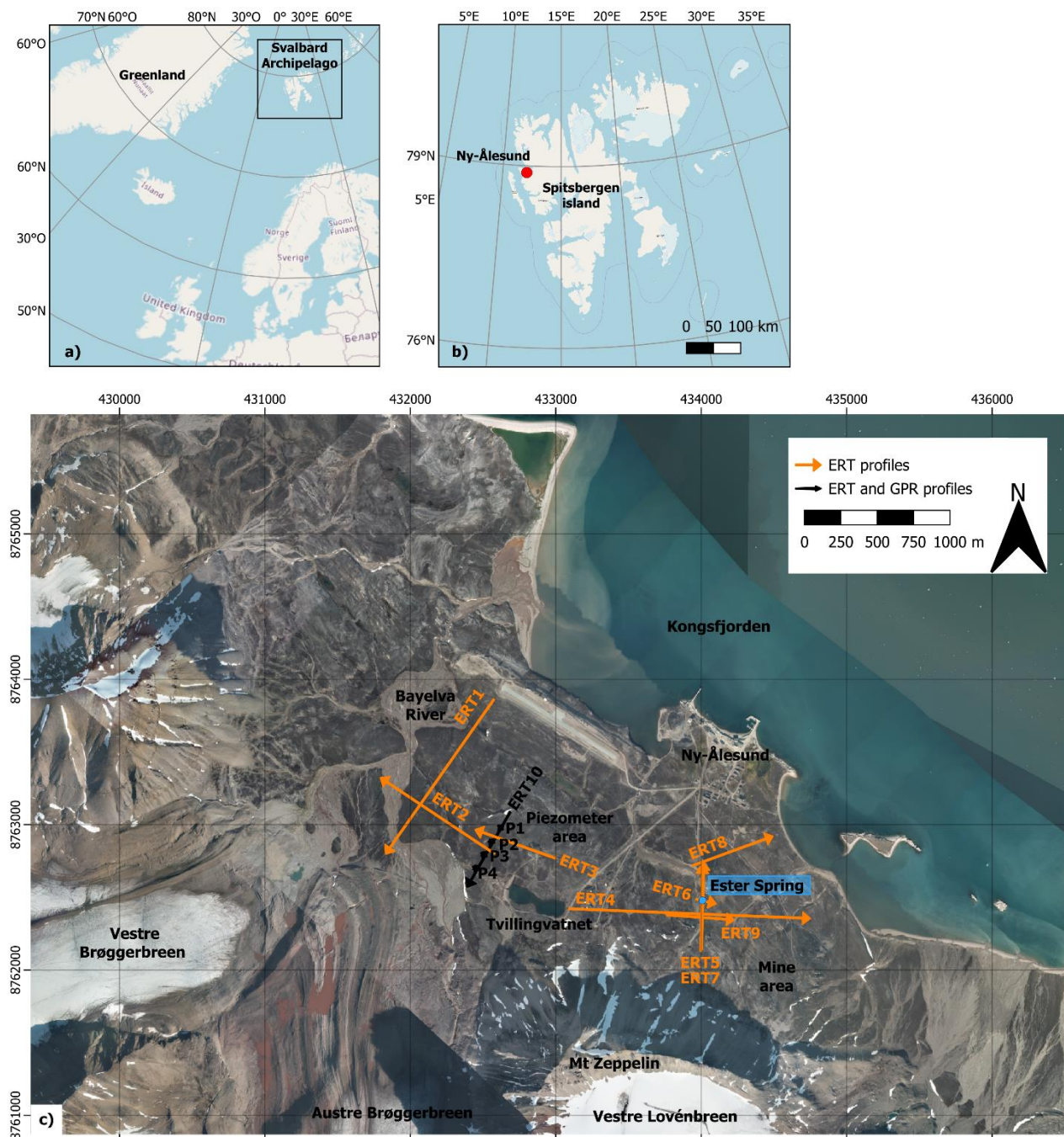
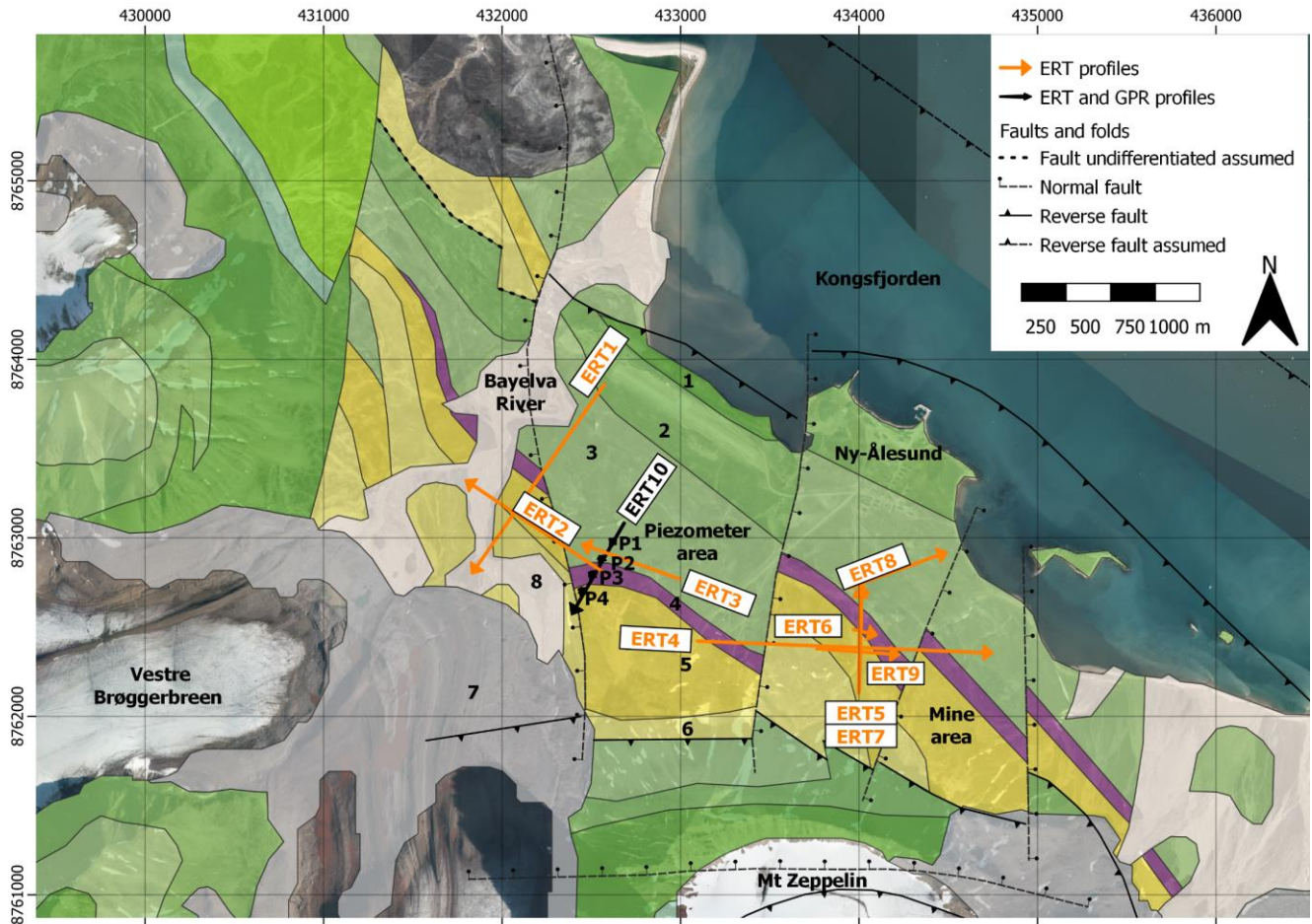


Figure 1: a) location of the Svalbard Archipelago; b) location of Ny-Ålesund on Spitsbergen, western Svalbard; c) a general overview of the area investigated by the ICeToFLUX project. The Ny-Ålesund settlement is close to the catchment of the Bayelva River. The orange lines represent the ERT profiles (from ERT1 to ERT10 and P1-P4). The black lines represent the profiles where both ERT and GPR were acquired. The coordinate system is WGS84-UTM33N. The satellite picture in background was exported from the WebGIS tool by ©Norwegian Polar Institute (<https://geokart.npolar.no/Html5Viewer/index.html?viewer=Svalbardkartet>)

). Some of the acquisitions overlap fully or partially: two surveys were performed in July-August 2022 and in August-September 2022, to possibly find some variations over time.



200 **Figure 2: Geological map (data from NPI, WMS geological map at 1:250.000): 1) Carbonate rocks of Wordiekammen Formation (Moscovian-Sakmarian); 2) Carbonate rocks of Gipshuken Formation (Sakmarian - Artinskian); 3) Chert, shale, sandstone and limestone of Kapp Starostin Formation (late Artinskian - Late Permian); 4) Shale, siltstone, sandstone of Vardebukta Formation (Induan); 5) Sandstone, shale, coal of Kongsfjorden Formation (paleocene ?); 6) Sandstone, shale, conglomerate of Brøggerbreen Formation (Paleocene?); 7) Moraine (Holocene); 8) Glacio-fluvial deposits (Holocene); NF) Normal fault; RF) Reverse fault. The coordinate system is WGS84-UTM33N. The geological map was exported from the WebGIS tool by ©Norwegian Polar Institute (<https://geokart.npolar.no/Html5Viewer/index.html?viewer=Svalbardkartet>).**

205

3 The geophysical survey

3.1 The ERT and GPR methods

ERT is an active geophysical technique that involves the injection of current into the subsoil, and the measurement of the consequent voltage distribution at the surface. The current is injected in a dipole of electrodes, called transmitter or source, while the voltage is measured at one or multiple dipoles, called receiver(s). The measured voltage is influenced by the

210

current flowing in the subsoil, which is, in turn, dependent on rock types, porosity, water saturation, salinity and temperature, weathering, metallic content, and clay content. The transmitter and the receivers can be placed in several relative positions or configurations. Different configurations are sensitive to different patterns of resistivity distribution. In the Ny-Ålesund survey, three configurations were employed: Wenner (WE), Wenner-Schlumberger (WS) and Dipole-Dipole (DD). While WE and WS are sensitive to the vertical layering of the subsoil, DD is sensitive to lateral resistivity contrasts (Martorana et al., 2017). The distance between the electrodes affects the depth of investigation of a measurement, the vertical penetration of the injected current, the lateral resolution of the data and the field logistic. The more the electrode spacing, the more the depth of investigation and the less the data resolution in the near surface (Oldenburg and Li, 1999). We chose the electrode spacings of 1 and 2 m to characterize the region of the active layer, and of 10 m to characterize the expected permafrost layers or deep aquifers, at the expense of high resolution in the near surface.

GPR is a non-invasive methodology that detects electromagnetic (EM) impedance contrasts in a medium. It is based on the analysis of the reflections of electromagnetic waves transmitted into the ground depending on the frequency of the electromagnetic waves and the electrical characteristics of the potential targets and surrounding soil (electrical permittivity and conductivity). The use of different antennas and frequencies enables the imaging of subsoil at different penetration depths: the lower the frequency the larger the penetration depth. Therefore, the operating frequency is always a trade-off between resolution and penetration depth. In our survey, the GPR acquisition was planned to retrieve high-resolution information at a relatively shallow depth. Two antennas with different frequencies were adopted: 400 MHz and 40 MHz. The emitted signal at high frequency (400 MHz) allows detailed information up to four meters of depth, that is enough to image the expected interface between the active layer and the permafrost. The 40-MHz signal was planned to reach 10-20 m of depth (Jol, 2009).

3.2 The MT method

The MT method is a natural-source electromagnetic method that measures the Earth's response to the low-frequency EM waves coming from the magnetosphere and ionosphere. The measurement of the electrical and magnetic fields allows determining the electrical resistivity of the Earth at depths ranging from some meters to hundreds of kilometers (Chave et al., 2012). The acquisition of MT data is performed with no transmitters since the signal has a natural origin. Two horizontal components of the electric and magnetic fields are measured on the ground surface. The electric field is measured by means of two pairs of dipoles (grounded non-polarizable electrodes), being usually the direction of one pair parallel to the magnetic North (x-direction for MT convention). The magnetic field components are usually measured by means of two horizontally buried magnetometers (induction coils). A third additional magnetometer can be deployed to measure the vertical component of the magnetic field.

The Audio-MT method (AMT) refers to the measurements of MT signals in the frequency range from 10^5 to 10 Hz. AMT is devoted to the shallow characterization of geoelectrical structures. The broadband MT method refers to measurements of both low and high frequencies usually in the range of 10^3 to 10^{-4} Hz with deeper investigation depths than AMT.

245 For our geophysical survey, two different systems were adopted for AMT and broadband MT acquisitions. The AMT equipment was composed of the Geometrics StrataGem system, two G100K magnetometers and four steel electrodes. The broadband MT equipment was tailored by Zonge International Inc. and consisted of one ZEN receiver (high-resolution, multi-channel 32-bit receiver), that records broadband time-series from 10^3 to 10^4 Hz, three magnetometers (type ANT/4) and six non-polarizable electrodes (Pb-PbCl) devoted to geophysical resistivity measurements.

250 The MT and AMT surveys were planned to be carried out during the I2F project because they have different resolution and depth of investigation with respect to ERT and GPR. MT and AMT were deemed to be ideal for the deep characterization of permafrost and sub-permafrost aquifers since they are more sensitive than ERT and GPR to electrically conductive formations and have a larger depth of investigation than ERT and GPR. Moreover, the MT and AMT methods were supposed to overcome the possible difficulties of the ERT method related to the injection of a direct current into a highly
255 resistive subsoil like that expected in Ny-Ålesund. There are several MT and AMT applications that study the ice sheet and glacial dynamics in the polar regions (Hill, 2020), both Arctic (Beka et al., 2015, 2016, 2017a, b) and Antarctic regions (Wannamaker et al., 1996, 2017).

The MT and AMT surveys were planned in the Bayelva and mine areas, but every attempt of acquisition had no success. The planned MT and AMT surveys had to be stopped after the acquisition of 5 soundings due to an unexpected high level of
260 anthropic electromagnetic noise. The first MT acquisition was scheduled with three different sampling rates for a total of 2.5 hours. The estimated impedances ranged in the frequency band from 0.01 to 1280 Hz but were affected by noise. Then, four AMT soundings were acquired, but – again – the data were corrupted by noise. The AMT time series were processed by using different window lengths and filtering stages in three frequency bands resulting in impedance estimates in the frequency range from 15.8 Hz to 63 kHz.

265 The MT data would have been useful for the deep characterization of the permafrost and potential sub-permafrost aquifer. However, the MT and AMT data processing performed after the first acquisition revealed a wide-band and energetic noise source whose presence prevented the possibility of acquiring good-quality MT data. This was completely unexpected because Ny-Ålesund is a radio silent and geographically remote settlement, where wireless equipment is not allowed to ensure a high signal-to-noise ratio for the data measured. Even though any equipment emitting radio signals is avoided and
270 several scientific instruments take advantage of the radio silence, a few exceptions are permitted for safety, operational and scientific reasons. The equipment transmitting and receiving radio frequencies in Ny-Ålesund is supposed to be authorized and listed in the “NySMAC frequency list” (<https://nyalesundresearch.no>). Although the listed equipment operates in the frequency range from kHz to GHz, it directly or indirectly affected the quality of our acquired MT signals in the frequency bands > 1 Hz. As an example, this low quality can be appreciated from Fig. 3, where the power spectra are dominated by a
275 50-Hz noise and its harmonics. The signal in Fig. 3 was analyzed in Matlab® Signal Processing Toolbox. The presence of this kind of noise resulted in the impossibility of obtaining reliable MT estimates. Note that in Fig. 3 the time series of the magnetic components are not deconvolved for the instrumental response.

Therefore, the MT and AMT surveys were shut down and the data were not included in the repository published along with this work due to the impossibility to process and interpret them. However, our experiment can be of help for future geophysical expeditions in Ny-Ålesund.

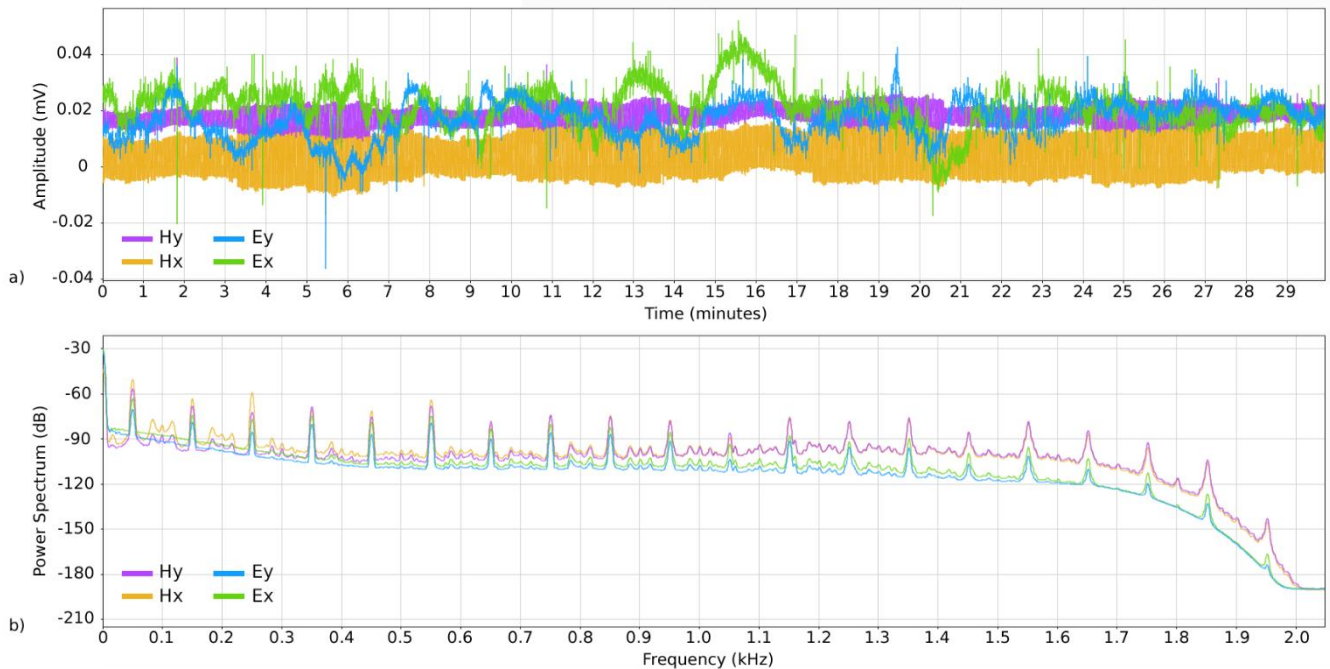


Figure 3: Time series (a) and power spectra (b) related to the Electric (E_x and E_y) and Magnetic (H_x and H_y) field components sampled at 4096 Hz. E_x is plotted in ochre, E_y in purple, H_x in green and H_y in cyan. The components were measured in the (magnetic) N-S and E-W directions. The signal was analyzed in Matlab® Signal Processing Toolbox.

285 3.3 Data acquisition

Three different sectors around Ny-Ålesund were surveyed (Fig. 2): i) the Bayelva catchment on the west, ii) the piezometer area close to the Amundsen-Nobile climate change tower (CCT), and iii) the mine area on the east (close to the Ester Spring).

The geophysical survey had to be planned to overcome some specific logistic difficulties owing to the study area placed in a remote polar region and to the long duration of the survey, split into two different campaigns during the thaw season. First, the whole equipment (14 boxes with a total weight of around 450 kg) had to be shipped two months before the survey and returned back three months after the survey ended. Second, the whole crew had to obey the health and safety protocols, required, respectively, to be hosted in the Italian Arctic Station and to carry out field operations in a region where polar bears may approach humans. Globally, field logistics and fieldwork conditions were largely affected by the isolation and asperity of the study area. For example, most of the survey sectors were not directly accessible from the road and hiking with the

equipment was necessary. Moreover, since safety was of primary concern, operators had to work nearby to monitor the presence of wildlife (polar bears) in the surroundings, thus extending the time required for the surveys.

The ERT survey was divided into two campaigns between July and September 2022. The instrument was the georesistivimeter Syscal Pro (Iris instruments). The receiver was multichannel with a maximum of 10 measurements at a
 300 time and a maximum number of 48 electrodes for each acquisition. Standard stain steel electrodes were used. The configurations of the acquisition were DD (both in direct and reverse configurations), WS and WE. The acquisition was usually moved forward by using the roll-along technique. The acquisition settings of the instruments were an injection time of 500 ms and a number of minimum 3 up to 6 stacks. The accepted error percentage on the stacks was 2%. A total length of 7.87 km was acquired along 18 profiles (Fig. 1c and Table 1). The electrode spacing was 10 m for 9 profiles (deep ERTs), 1
 305 m for 8 profiles and 2 m for the remaining one (shallow ERTs). The details about the acquired ERT profiles are schematized in Table 1.

The soil conditions were generally fair in terms of electrical contact resistance, allowing to easily achieve contact resistance values lower than 10 k Ω . This was not surprising because the thaw season is generally the best season for ERT data quality since the contact resistances are expected to be low (Herring et al., 2023). Not favorable conditions were encountered in
 310 areas where stones and gravels covered the ground surface, such as in the Bayelva catchment and in the mine area. The bentonite was used there to improve the ground-electrode contact, if necessary. For some of the profiles the contact resistance values were stored together with the data to enhance a posteriori control of the data quality (see Section 4.1). The contact resistance was stored only for the WS acquisitions due to the negative influence that this procedure has on the multichannel acquisition (i.e., the DD acquisition) in terms of time consumption.

315 **Table 1: Data acquisition parameters and array configuration for ERT profiles. The coordinate system is WGS84-UTM33N.**

Name	Length (m)	Spacing (m)	Arrays	Roll Along	East – 1st electrode	North – 1st electrode	East – last electrode	North – last electrode
ERT1	1310	10	DD, WS	7	432575	8763862	431830	8762798
ERT2	950	10	DD, WS	4	432577	8762801	431794	8763323
ERT3	590	10	DD, WS	1	432997	8762768	432446	8762965
ERT4	1670	10	DD, WS	10	433091	8762422	434750	8762355
ERT5	590	10	DD, WS	1	433998	8762128	434009	8762718
ERT6	142	2	DD, WS	2	433965	8762488	434102	8762456
ERT7	590	10	WE, WS, DD	1	433997	8762124	434012	8762710
ERT8	590	10	WE, WS, DD	1	433936	8762703	434483	8762899
ERT9	470	10	WE, WS, DD	0	433763	8762384	434227	8762341
ERT10	590	10	WE, WS, DD	1	432674	8763075	432383	8762567
ERT_P1_Ort	47	1	WS	0	432602	8762986	432637	8762962

ERT_P1_Par	47	1	WS	0	432625	8762993	432602	8762952
ERT_P2_Ort	47	1	WS	0	432536	8762881	432580	8762871
ERT_P2_Par	47	1	WS	0	432563	8762896	432542	8762854
ERT_P3_Ort	47	1	WS	0	432486	8762800	432526	8762775
ERT_P3_Par	47	1	WS	0	432516	8762806	432491	8762767
ERT_P4_Ort	47	1	WS	0	432429	8762708	432470	8762683
ERT_P4_Par	47	1	WS	0	432460	8762715	432437	8762675

The two 10m-spacing profiles in the Bayelva catchment (ERT1 and ERT2) are perpendicular and very close to the Bayelva River, that is crossed at the end of the two ERTs toward the glaciers. In the area of the piezometers, there are two perpendicular 10m-spacing profiles (ERT3 and ERT10) and 8 short profiles (1m-spacing) that cross the four piezometers (P1, P2, P3, P4) in parallel and orthogonally. Then, the mine area is crossed by the longest line ERT4 (1.67 km), which partially overlaps ERT9. Three profiles cross the Ester Spring (ERT5, ERT6, ERT7) and a profile is directed towards the sea (ERT8). ERT7 and ERT5 are partially coincident because they were measured during two different campaigns, in July and September 2022, respectively. The same applies to ERT9 and ERT4, respectively. ERT6 was acquired with 2m-spacing.

The GPR data were acquired with the GSSI SIR-3000 GPR System coupled with two different antennae working at the frequencies of 40 MHz (SUBECHO AB Sweden air-coupled antenna) and 400 MHz (GSSI ground-coupled antenna). The adopted recording time window is set to 120 ns for the acquisition performed with the 400 MHz antenna and 1200 ns for the data acquired with the 40 MHz antenna. The acquired data were discretized by 512 time-samples. Since the acquisitions were carried out without a survey wheel, the data were acquired in time domain and several marks were placed every 5 meters in order to assign the right coordinates to each recorded trace. The GPR survey was carried out in the piezometer area, as shown in Fig. 2. The cumulative surveyed length is about 1400 meters along 10 GPR lines. Each line has been measured in a direct and reverse sense for a total surveyed length of 2800 meters. The 400 MHz antenna was used to measure GPR radargrams along the 8 shallow ERT profiles centered in the four piezometers (P1, P2, P3, P4) and along the ERT10 line crossing all the piezometers. The antenna at 40 MHz was adopted for a line in correspondence of ERT10. The details about the acquired GPR profiles are schematized in Table 2.

The surface investigated close to the piezometer area was regular and the few ground irregularities encountered did not affect the quality of the acquired data, always ensuring a proper surface contact for the ground coupled antenna. The use of the 400 MHz antenna was limited to transect line where it was possible to guarantee and adequate contact between the ground and the antenna avoiding unwanted “jumps” of the antenna itself. This limitation was not affecting the use of the 40 MHz antenna which performs well even in absence of direct contact with the ground.

Table 2: Data acquisition parameters for GPR profiles.

Name	Length (m)	Frequency (MHz)	East – starting profile	North – starting profile	East – ending profile	North – ending profile
-------------	-----------------------	----------------------------	------------------------------------	-------------------------------------	----------------------------------	-----------------------------------

GPR_P1_Ort	50	400	432602	8762986	432638	8762960
GPR_P1_Par	50	400	432625	8762993	432600	8762950
GPR_P2_Ort	50	400	432536	8762881	432583	8762870
GPR_P2_Par	50	400	432563	8762896	432539	8762851
GPR_P3_Ort	50	400	432486	8762800	432529	8762773
GPR_P3_Par	50	400	432516	8762806	432489	8762764
GPR_P4_Ort	30	400	432429	8762708	432455	8762692
GPR_P4_Par	28	400	432460	8762715	432446	8762690
GPR_Long_40MHz	590	40	432674	8763075	432383	8762567
GPR_Long_400MHz	445	400	432447	8762693	432642	8763023

340 4 The data set

4.1 Raw data and quality control

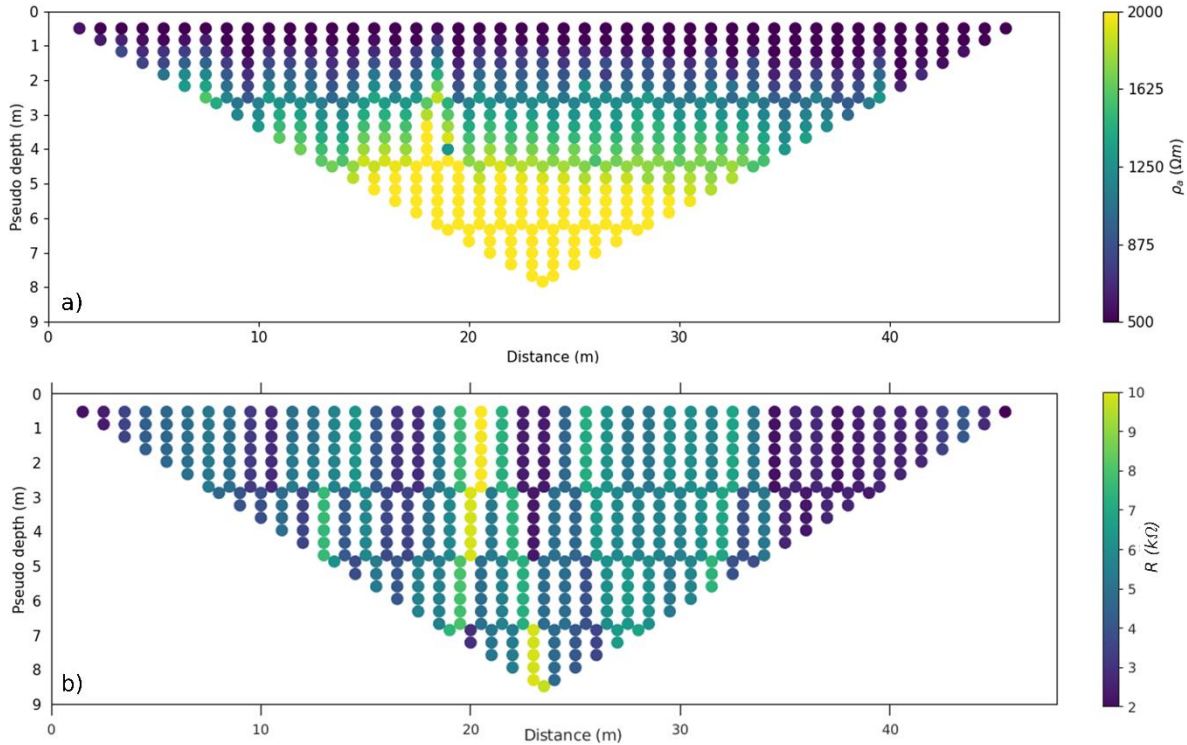
As standard practice, each acquisition of ERT data was preceded by the check of the contact resistance between the electrodes and the ground. This operation (“RS check”) was directly performed by the instrument. As an additional quality control (QC), specific electrodes (occupying a known position along the geoelectrical lines) were unplugged before starting
345 the contact resistance check in order to verify the correct number addresses of the electrodes. When one of the unplugged electrodes was involved in the RS check, the georesistivimeter stopped the check operation as long as the electrodes were correctly plugged. The contact resistance values of ERT7, 8, 9,10 and ERT_P1, P2, P3, P4 were stored together with the WS geoelectrical data to enhance a posteriori QC and monitoring of the measuring conditions.

At the end of each ERT survey, an in-field evaluation of the collected data quality was performed. The data were
350 downloaded from the georesistivimeter and visualized as pseudosections of apparent resistivity (see for example Fig. 4a). The regularity of the data distribution in relation to the measuring conditions was used to drive decision-making on the necessity of repeating the data acquisition or changing the investigation strategy.

Noisy data in the geoelectrical measurements can be due to soil conditions, complex subsoil structures or instrumental failure. Soil conditions can negatively affect the ERT data if the ground-electrode electrical contact is not ideal. This
355 condition is common in those areas where stones and gravels cover the ground surface, such as in the Bayelva catchment and in the mine area. Bentonite was used to improve the ground-electrode contact when needed.

The QC on the field for the GPR data was aimed to verify the proper functioning of the GPR acquisition system (control unit and antennas) and the correct settings of the acquisition parameters (time window, sampling rate, gain, trace increment, etc.). The QC was preliminarily done, during the data acquisition process, directly on the GPR acquisition system monitor.

360 Subsequently, a more thorough verification was performed in the lab after the acquisition, resulting in the elaboration of preliminary 2D radargrams.



365 **Figure 4: Example of experimental pseudosection of the ERT_P1_Par profile. The acquisition configuration is WS: a) spatial distribution of the measured apparent resistivity (ρ_a) values (in Ωm); b) contact resistance values (in $\text{k}\Omega$) recorded for each pair of current electrodes involved in the data acquisition sequence.**

4.2 The processed data

The ERT data were pre-processed by using the software Prosys-III (Iris instruments). The filtering procedure of ERT data was based on the verification of some general criteria. For each geoelectrical profile the preprocessing consisted of discarding the following data:

- 370
- electrodes with anomalous values of contact resistance (“RS check”), when available,
 - negative resistivity values,
 - isolated extremely high or low resistivity values (i.e., outliers).

An example of ERT data with the pseudosections of apparent resistivity and contact resistance with a WS configuration is depicted in Fig. 4 for profile ERT_P1_Par. It is centered at piezometer P1 and is parallel to ERT10. This profile was chosen as representative since GPR data were acquired at the same location (see Section 5.2). The apparent resistivity pseudosection (Fig. 4a) is characterized by relatively smooth variations and no outlier data as expected considering the good contact resistances (Fig. 4b). The filtered ERT data were then ready to be inverted to create 2D geoelectrical models of the subsol

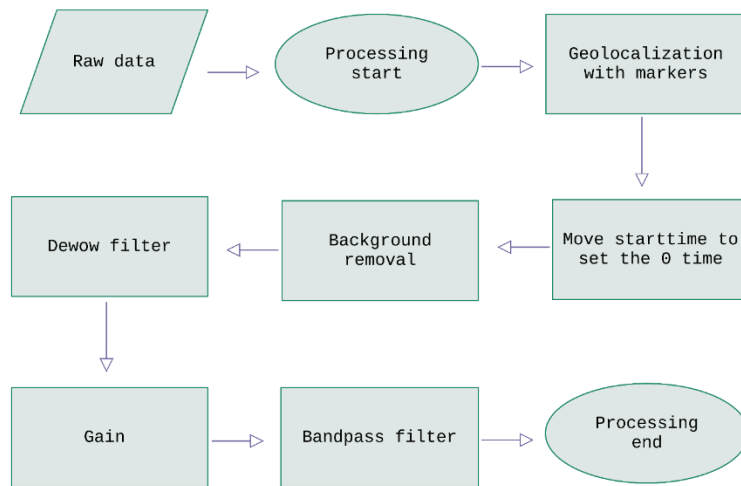
375

(see Section 5.1). The whole set of pseudosections measured along each ERT is presented in the repository (see Section 6 for details).

380 The GPR data were processed with Reflexw software (Sandmeier, 2021), according to the processing chain depicted in Fig. 5 and accurately explained:

- the distance between each trace was set in order to match, every 5 meters, the geolocation of the marker, with the "marker interpol." processing step;
- a time-zero correction was performed, with the "move starttime" processing step, by manually selecting, as time
385 zero, the value in nanoseconds correspondent to the beginning of the transmitted impulse;
- a background removal filter was applied over the whole profile, subtracting the average trace from each trace;
- a subtract-mean, or "dewow" filter, was used with a time window of 2 ns and 8 ns for 400 MHz and 40 MHz data, respectively, to remove possible instrumental voltage shift in the data;
- a manually selected gain function, based on the operator's choice and experience, was applied to contrast the
390 effects of signal attenuation and geometric dispersion;
- a bandpass filter removed the frequencies below about 150 MHz and above about 550 MHz for 400 MHz data and between 20 and 100 MHz for 40 MHz data;
- only for the 40 MHz data, an automatic gain control (AGC) with a time window of 100 ns was applied in order to better detect deep reflectors.

395 For visualization, the topography of all GPR data was corrected by using the topographic surface retrieved from a recent Digital Elevation Model with 5 meters of resolution, published by the Norwegian Polar Data Centre and available as basemap data "Svalbard digital elevation models" at <https://geodata.npolar.no> (©Norwegian Polar Institute, 2014). Each radargram was normalized to its amplitude mean value.



400 **Figure 5: GPR processing flow adopted for the GPR lines of the ICEtoFLUX project.**

5 Representative results

5.1 ERT inversion method

The ERT data pre-processing and filtering of the outliers is usually followed by the geophysical inversion of the acquired data. The inversion aims at finding the best resistivity distribution of an Earth model which explains the data within a certain error threshold.

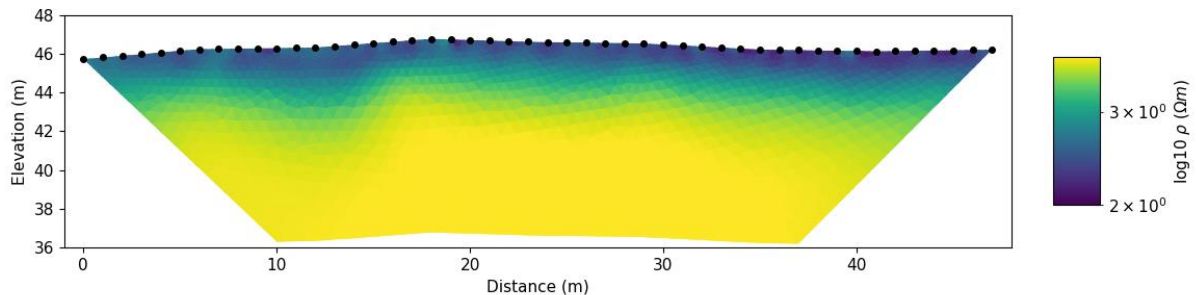
The 2D ERT inversion was performed by using the open-source package ResIPy (Blanchy et al., 2020). ResIPy can be used for geoelectrical data (direct-current and induced polarization measurements) and provides several tools such as high-level filtering, error modelling, 2D and 3D inversion/forward modelling and post-processing. It can be accessed from a Python application programming interface (API) or a standalone graphical user interface (GUI). Further information about ResIPy and other software for electrical resistivity modelling can be found in Doyoro et al. (2022) and Loke et al. (2013).

In the inversion process, the same mesh discretization was adopted in terms of cell growing factor, characteristic length, and background resistivity. The boundary depth of the model was 80 m for the ERT lines with 10 m of spacing between the electrodes. The cell growth factor was 7. The characteristic length was kept as the ResIPy default to ensure two mesh nodes between two consecutive electrodes. The topography was included. The inversion type was a regularized inversion with linear filtering and normal regularization. The same inversion settings were adopted for all the quadrupole configurations (WE, WS, DD). The only exception was for the measurement errors given to the inversion. For the WE and WS data sets, the data error was set to 2%, in agreement with the largest observed stacking errors. For the DD data sets, an ad hoc error model (linear or power law) was calculated from reciprocal error distribution and then used in the inversion procedure.

The number of iterations was between 2 (for short profiles) and 10 (e.g., for the longest ERT4), all computed in few seconds.
420 The final root-mean-square errors (RMSEs) ranged between 1 (the minimum threshold to end the inversion) and 2.18 (for ERT4, which had high errors).

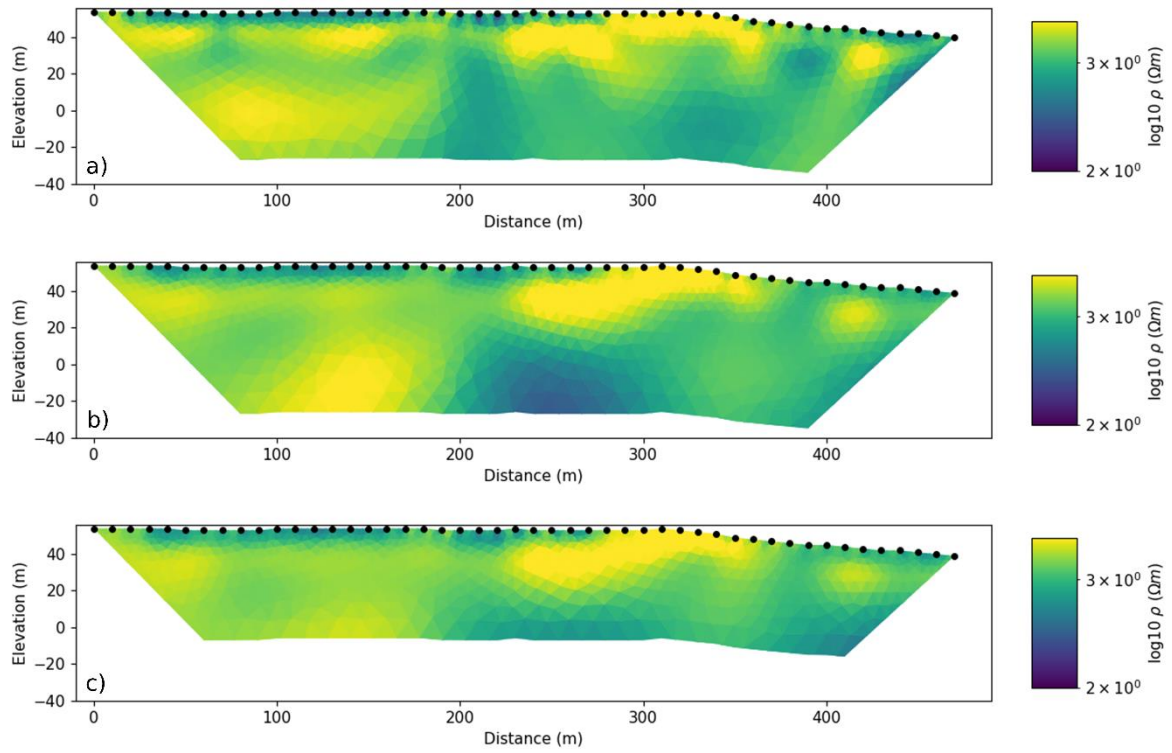
5.2 The ERT models

The inversion result for the ERT_P1_Par (WS configuration, 1 m of electrode spacing) is presented in Fig. 6. The resistivity model shows a gradual increase in resistivity with depth. At shallow depth, up to 2 m of depth b.g.l., the resistivity range is
425 100 – 500 Ωm , while from 2 m of depth down to the bottom of the model the resistivity rises to 1000 Ωm and even up to 8000 Ωm , which can be theoretically correlated with the permafrost. The resistivity model of Fig. 6 does not show a marked lateral variability, that is, the resistivity clearly increases with depth, being characterized by a shallow medium resistive layer and a deep very high resistive layer. This geoelectrical structure is valid for only profile ERT_P1_Par because the measured apparent-resistivity data in the ERT profiles centered in the other piezometers are clearly different. Further interpretation of
430 the resistivity models goes beyond the scope of this paper and needs multidisciplinary contributions, given that the resistivity of the frozen rock might be site-specific. To the best of the authors' knowledge there is no direct measurement of electric resistivity in the investigated area, except for few, old and superficial electric-conductivity sensors installed up to 1 meter of depth in the Bayelva basin (Kodama et al., 1995; Boike et al., 2018; Son and Lee, 2022).



435 **Figure 6: Resistivity model obtained from the inversion of ERT_P1_Par. The acquisition configuration is WS. The minimum and maximum boundaries of the color bar are 100 and 3000 Ωm , respectively.**

Another representative example of results is ERT9, that was acquired with 10 m of electrode spacing and with different quadrupole configurations (DD, WS, WE). ERT9 is located in the mine area and close to Ester Spring. The inversion results for ERT9 are presented in Fig. 7. The general picture presented by the three models is basically the same, but the DD (Fig.
440 7a), having a higher lateral sensitivity and data coverage, offers a more resolved picture of the underlying electrical structure. Among the three models, the less informative one seems the WE (Fig. 7c), which is highly resembling the WS model (Fig. 7b), but with low resolution in terms of spatial data coverage and array characteristics. The reliability of the inversion results is derived not only from the similarity of the three geoelectrical models of Fig. 7, but also from the pseudosections of the contact resistance (stored with the WS data), as shown in Fig. 8a, and of the percentage reciprocal error (derived by
445 measurements in DD direct and reverse configuration), as shown Fig. 8b.



450 **Figure 7: Resistivity model obtained from the inversion of ERT9. Different acquisition configurations: a) DD; b) WS; c) WE. The minimum and maximum boundaries of the color bar are 100 and 3000 Ωm , respectively.**

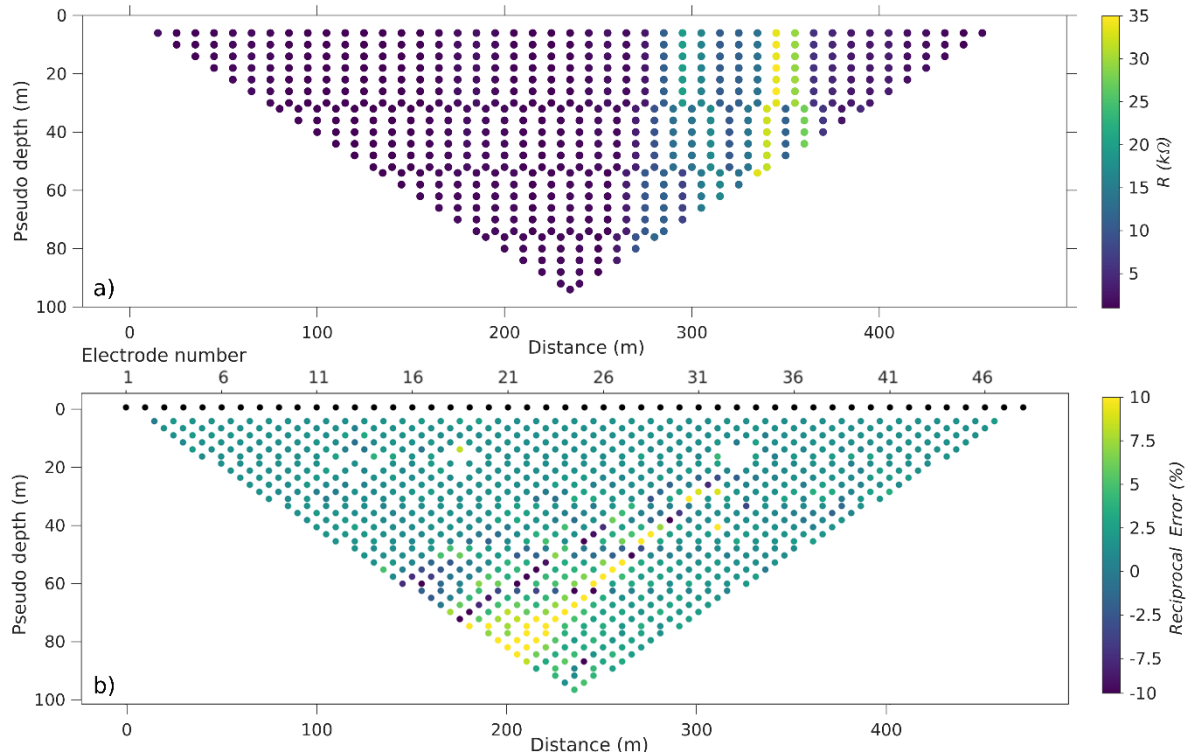


Figure 8: Pseudosections of ERT9 for: a) contact resistances stored during the WS acquisition; b) percentage reciprocal errors derived from the DD acquisitions performed in direct and reverse configurations.

455 As regards the quality of the ERT data, different levels of noise and error were recognized. For example, Fig. 8b represents for ERT9 the pseudosection of the percentage reciprocal errors that are in the range $\pm 2.5\%$ for most of the data points and reach $\pm 10\%$ for some of them at 60-90 m of pseudodepth. The pseudosections from the Bayelva catchment presented reciprocal errors up to $\pm 40\%$ (see in the repository the figures “ReciprocalError.png” in folders **2_Filtered_data_inversion_input/DD**). In contrast, the pseudosections of the percentage reciprocal errors in the piezometers area showed the lowest values, with a maximum of $\pm 4\%$ (for example, see in the repository ERT10, DD acquisition). Given that the quality of ERT data was heterogeneous among the different profiles, the data set provided in the repository includes the raw data as well as processed/filtered ERT data ready to use. The raw data can be inspected for each line to allow the user assessing the original measurement errors (stacking errors) or the reciprocal errors and then potentially reprocessing them according to different criteria.

465 The post-processing analysis of the inversion results was carried out in Matlab[®], where we imported the ResIPy output (that is, the file “f001_err.dat”) to plot the spatial distribution of apparent resistivity (observed and calculated) and the errors. The Matlab script to generate this kind of figure is provided in the repository for reproducibility, in the folder “*ERT/Example results*”, under the name “*Post_processing_Matlab.pdf*”.

Fig. 9 shows an example of post-processing for ERT_P1_Par (WS configuration). There is no topography in this kind of representation since the vertical axis is a pseudo-depth. The three panels illustrate the pseudosections of measured data (a), computed apparent resistivities (b) and the misfit between them (c). The pseudo-depth was calculated following Edwards (1977), that is, the same approach adopted in ResIPy (Fig. 4). The computed response is the apparent resistivity values that one would obtain performing a measuring operation on a subsoil in which the resistivity is distributed exactly as in the calculated resistivity model as in Fig. 6. The lower the misfit between the observed and calculated data, the more the reliability of the inversion result.

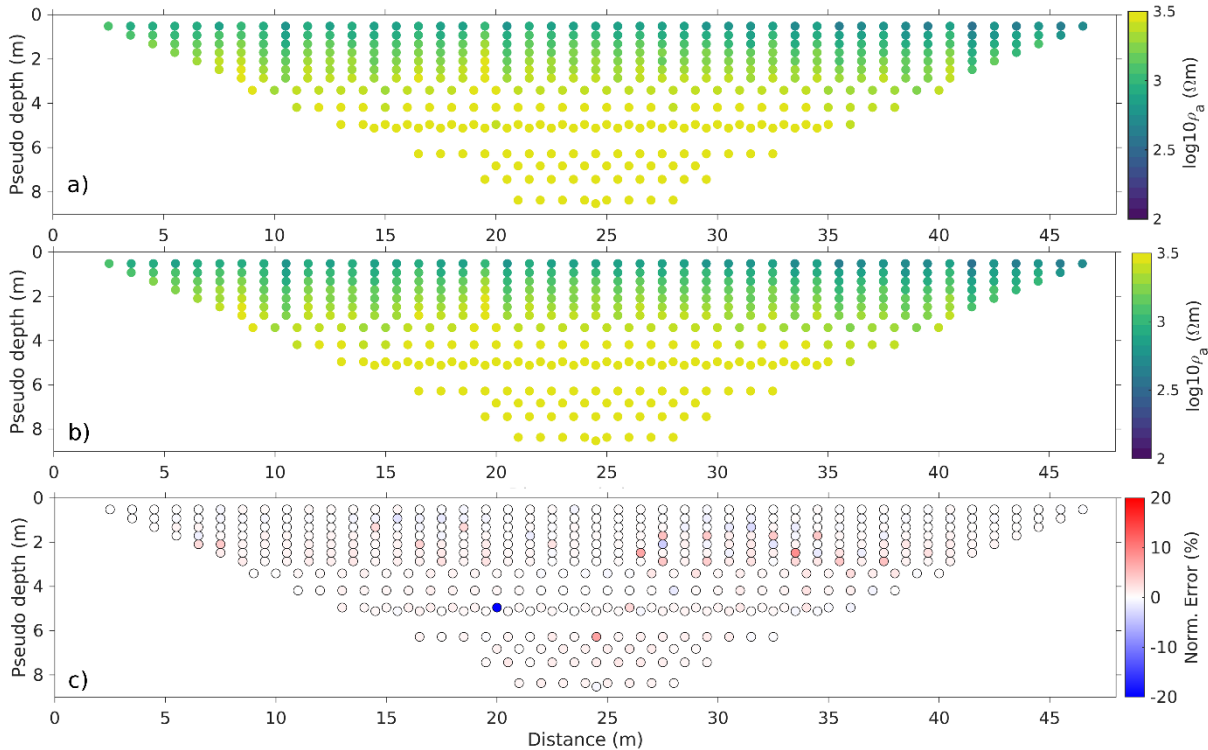


Figure 9: Post-processing analysis of the ResIPy inversion result for ERT_P1_Par, WS configuration: a) observed data (ρ_a); b) calculated response (ρ_a); c) misfit between them, calculated as normalized error in percentage.

5.3 The GPR results

Fig. 10 shows GPR_P1_Par, a representative GPR line that is parallel to ERT_P1_Par and acquired with the 400 MHz antenna. The radargram is acquired close to piezometer P1 and unequivocally shows the presence of a reflective layer placed in a time window ranging between 50 and 55 ns. In order to convert the data from the time domain to the spatial domain it is necessary to determine the propagation speed of the radar waves in the investigated levels. This is mainly related to the physical–electrical characteristics of the investigated medium. In particular, in a low-loss material, it is inversely proportional to the square root of the dielectric constant (ϵ_r) and is estimated or calculated through various possibilities of signal analysis or with experimental calibration tests. From the analysis and fitting of the hyperbolae characterizing the

radargrams (Rønning, 2023), generated by punctual elements present in the subsoil (i.e., stones), it was possible to determine that the velocity value can be assumed equal to 0.10 mns^{-1} . This assumption was also validated by the comparison of the most reflective layer detected by the GPR data with the most interesting electrical anomalies detected by ERT at a similar depth. Further efforts are required to constrain the interpretation with the direct data that will be collected in the close piezometer P1.

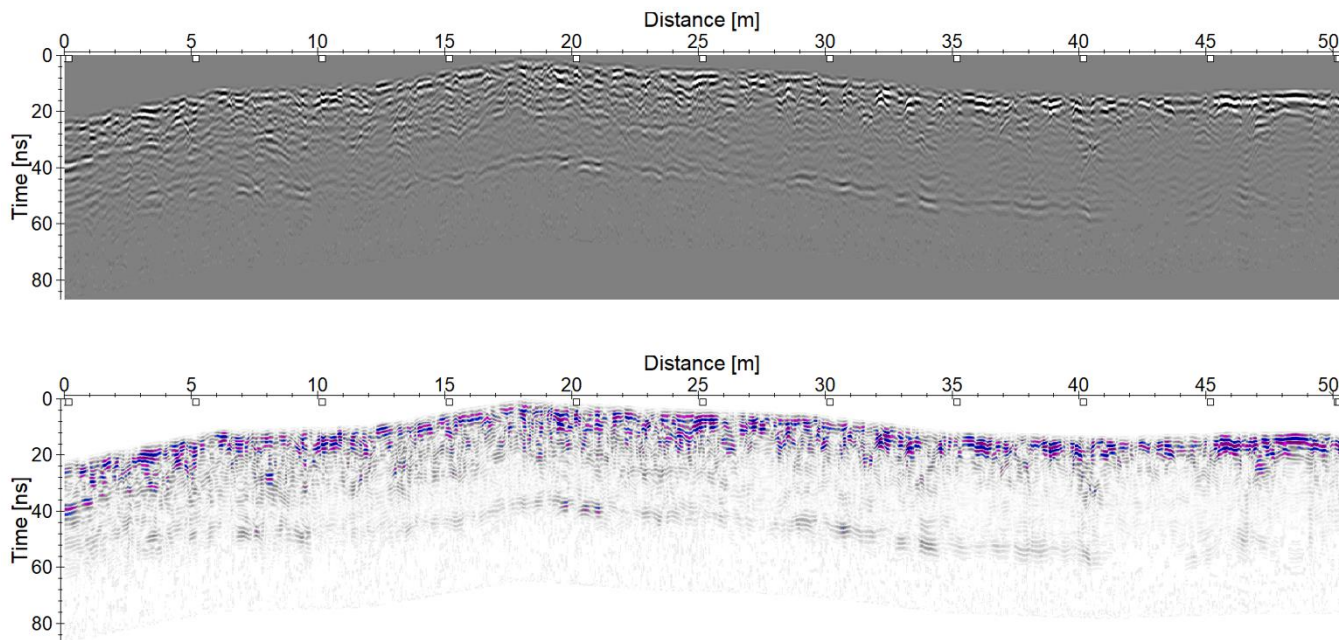
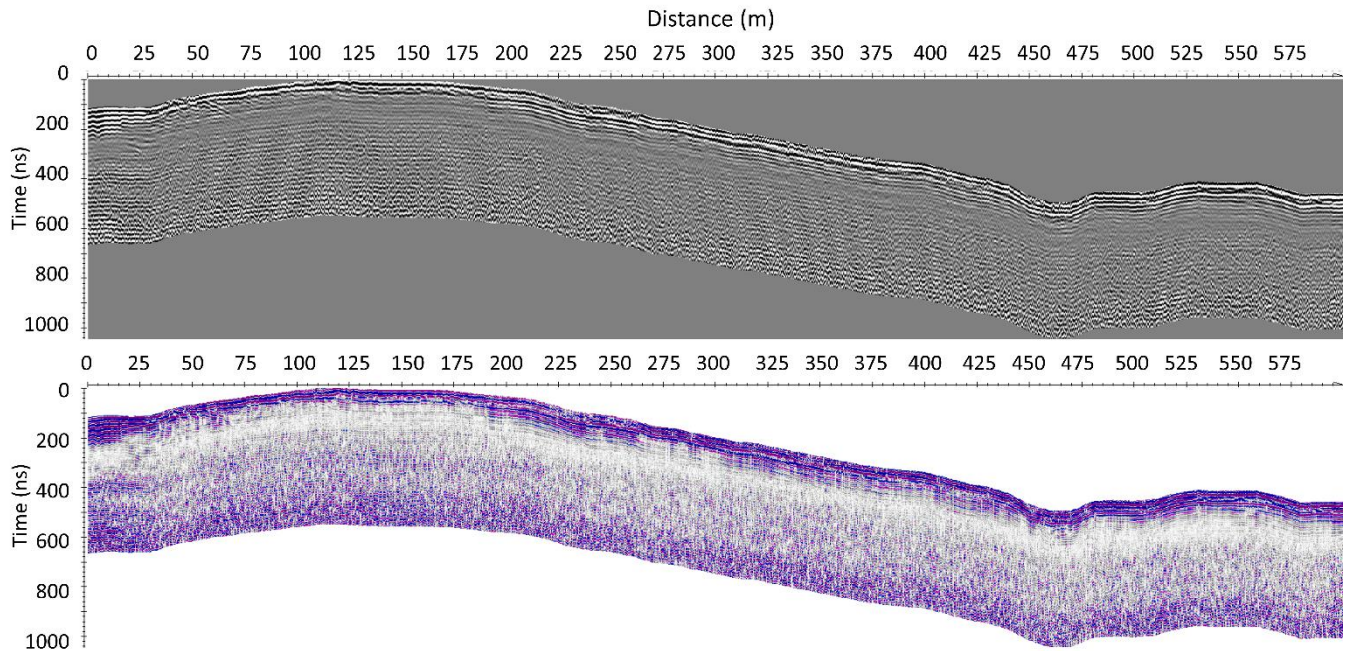


Figure 10: Example of a processed 2D radargram for GPR_P1_Par, which is parallel to ERT_P1_Par and was acquired with the 400 MHz antenna. The radargram is shown in two different color scales.

Fig. 11 shows the results obtained with the 40 MHz antenna for profile GPR_long_40 which is the only one acquired at low frequency. The radargram was acquired with an antenna that does not require ground contact. Although the recorded signal is noisier than that acquired with the 400 MHz antenna and the resolution is not comparable to that provided by the 400 MHz antenna, some reflective layers can be detected in the upper 300 ns. Later than this time, the presence of attenuation phenomena seems not providing the possibility of identifying hydrogeological features. However, some discontinuities seem to characterize the radargram in particular at 450 m of distance from the starting point of the radargram, where there is the Bayelva River. Even though Figs. 10 and 11 do not include the depth scale, all the processing details are provided in Section 4.2 for both antennas (40 and 400 MHz). The values for the processing reported in Section 4.2 can be applied to the GPR data acquired at 400 MHz as the presence of some hyperbolae allows the estimation of the EM wave velocity. The GPR data acquired at 40 MHz reach a depth of investigation significantly higher than that at 400 MHz. The absence of clear reflectors

505 (hyperbolae) and the scarce availability of prior hydrogeological information prevented the assumption of a single value for the migration of the radargram, which would have yielded an excessive simplification potentially inconsistent with the expected heterogeneity of the subsurface.



510 **Figure 11: Example of a processed 2D radargram for GPR_long_40 MHz radargram. The radargram is shown in two different color scales.**

6 Database publication of data and results

This section is mainly dedicated to the readers interested to download and reuse the data. The aim is to provide raw and processed data in formats that are friendly for geophysical software, in order to allow geoscientists to visualize them best, and reprocess them. We also provide the two representative inversion models shown in Figs. 6 and 7 as ready-to-use profiles of electrical resistivity of the subsoil, for scientists interested to directly use the results for multidisciplinary studies, e.g., to produce geologic or hydrogeologic models, and for comparison of different inversion schemes. The coupled data sets of ERT and GPR data along the 9 coincident profiles can also be used to test different joint inversion schemes.

6.1 Repository organization

520 The repository is organized in two main folders, as shown in Fig. 12: ***ERT*** and ***GPR*** (the folder names are highlighted in bold italic).

The subfolder *Data* in *ERT* contains 18 subfolders, one for each deep ERT (from *ERT1* to *ERT10*), and each shallow ERT close to the four piezometers (from *ERT_P1_Par/Ort* to *ERT_P4_Par/Ort*). With regards to the latter, the notations “Ort” and “Par” refer to orthogonal and parallel directions with respect to the ERT10 that crosses the piezometers, respectively. Schematic information about the ERT profiles is shown in Table 1. The scheme of the folder organization is depicted in Fig.

525 12.

Each of the 18 ERT folders contains the following subfolders:

- **1_Raw_data**: it contains .bin files, as saved by the Syscal Pro georesistivimeter. The .bin files contain the elevation information for each electrode and its relative position in the line. The files do not include the geographical East and North coordinates of the electrodes.
- 530 - **2_Filtered_data_inversion_input**: it contains a .Dat file which is the classical input format for performing the inversion in RES2DINV software (Loke, 2004; Loke and Barker, 1996), also readable by ResiPy. This folder contains the ResiPy project file (.resipy) with embedded the electrode coordinates, the topography, the mesh created for the inversion, the inversion settings and result. The folder stores a .png image of the pseudosection of the apparent resistivity. For *DD* surveys, the evaluation of the reciprocal error was calculated, that is, the difference
535 between resistivity measurements performed on the same quadrupole, but with transmitter and receiver electrodes switched. For *DD* surveys there are some supplementary files: a .csv file (“ErrorData.csv”) storing the calculated errors, a .Dat file (“#_rec_err.Dat”) that allows the ResiPy inversion to be performed by accounting the reciprocal errors, two figures (.png) that show the resistance error plot and the spatial distribution of the reciprocal errors.
- **3_Topography**: it contains a .csv file with columns representing the electrode number, East, North and altitude, in
540 Coordinate Reference System (CRS) WGS84, projection UTM, zone 33N (EPSG 32633). The East and North coordinates were collected during geophysical acquisition thanks to GPS measurements. We considered inadequate the accuracy of the altitude measurements by GPS, so the surface topography was retrieved from a 5-m digital elevation model (DEM) of the area openly provided by the Norwegian Polar Institute (©Norwegian Polar Institute, 2014, <https://geodata.npolar.no/>).

545 The three previous subfolders are organized according to the *Quadrupole configuration*, that is, in *WS* (Wenner - Schlumberger), *DD* (Dipole - Dipole) and, if measured, *WE* (Wenner).

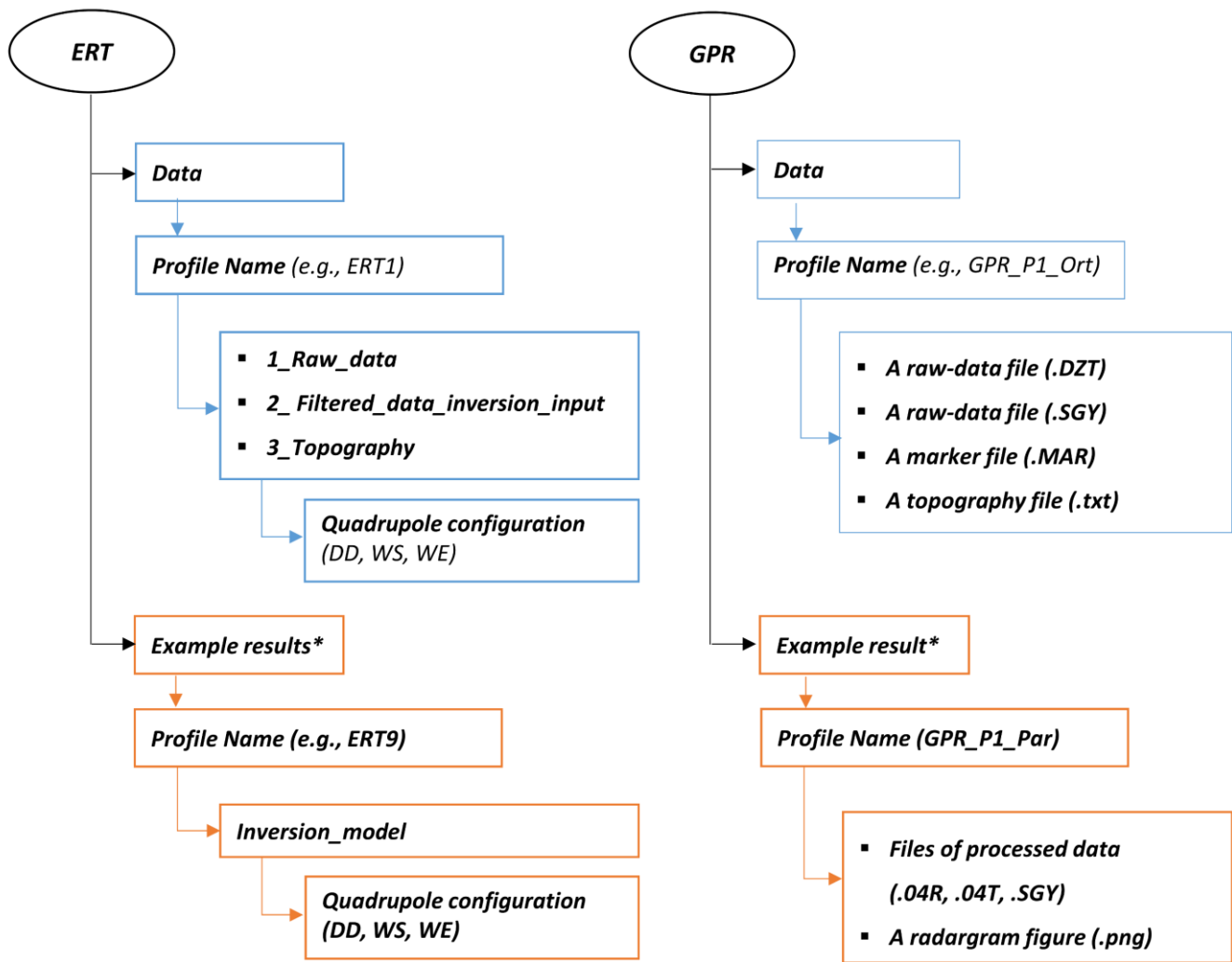
The repository stores some representative results of ERT 2D inversion for the two profiles shown in the Section 5.1 (i.e., *ERT_P1_Par* and *ERT9*). Their location in the repository is in folder *Example results* in *ERT*, where for each profile there is a folder *Inversion_model* (see Fig. 12). It contains, for each *Quadrupole configuration*, the result of the inversion, that is,
550 the sections of electrical resistivity of the subsoil, as shown in Figs. 6 and 7. The 2D resistivity models are provided as .png images for fast visualization (e.g., “Model.png”, “Misfit.png”, “NormErrors.png”), and .vtk files to allow further visualization processing in software like Paraview (Hansen and Johnson, 2005). Other relevant files in this folder are the “3plot.tif” file, which shows pseudosections of the measured and computed apparent resistivity and their difference (as in Fig. 9), and the mesh files .geo and .msh, readable by Gmsh software (Geuzaine and Remacle, 2009). The remaining files

555 (e.g., “electrodes.dat”, “protocol.dat”, “R2.out”) are automatically generated and saved by ResIPy and have the same name of the corresponding files saved by the freeware package R2 (Binley, 2023), whose manual is free to access.

The *Data* folder in *GPR* folder contains 10 subfolders (*Profile Name* in Fig. 12), one for each transect, 8 of which are coincident with the 8 shallow ERTs described above, and the other two are on the same path of ERT10 (i.e., *GPR_Long_40MHz* and *GPR_Long_400MHz*). The eight short GPR profiles were measured with a 400 MHz antenna and
560 centered in the four I2F piezometers. Schematic information about the GPR profiles is shown in Table 2. Each folder of GPR profiles contains four files (see Fig. 12):

- the original file of raw data in .DZT (Radan) format,
- the file of raw data in SEGY format (.SGY),
- the marker file (.MAR) that stores the number of the trace (first column) and the distance along the profile
565 (second column),
- the text file (.txt) for the topography, which contains the distance along the profile (first column), a second column of zeros and the corresponding elevation (third column).

Two examples of processed data are provided for profile *GPR_P1_Par* (Fig. 10) and profile *GPR_Long_40MHz* (Fig. 11), inside folder *Example_results* in *GPR*. The data were processed according to the workflow explained in Fig. 5 and saved in
570 Reflex-w format and in SEGY format (Hagelund and Levin, 2017). The files following the Reflex-w format are named “*GPR_P1_Par_processed.04(T-R)*” and “*GPR_Long_40MHz_processed.01(T-R)*”, while the remaining files are “*GPR_P1_Par_processed.SGY*” and “*GPR_Long_40MHz_processed.SGY*”. The processed files in Reflex-w and SEGY format have topographic correction. The image file is provided for fast visualization.



**Only for selected profiles*

575 Figure 12: The workflow of the repository of ERT and GPR data acquired in Ny-Ålesund.

6.2 Specifications of data file

In this section, the main file types used for sharing the ERT and GPR data are described.

6.2.1. ERT files

The apparent resistivity values are given in a text file with .DAT extension, according to the RES2DINV format (Loke, 580 2004). The data can be edited using any general-purpose text editor to check and manually modify the data file. The data are arranged in an ASCII delimited manner where a comma or blank space or LF/CR is used to separate different numerical data

items. The data format used here is a general array format, to include non-conventional arrays of any configurations. The data file .DAT is organized in three different slots: the headers, the apparent resistivity section, and the topographical section. The headers include the flag of the configuration array, the number of apparent resistivity data and other information
585 on the transect. The data are organized in nine columns: the x and z coordinates of the four electrodes for each sequence and the column of apparent resistivity (in Ωm). Additional information and details about how the data files are structured are reported in the RES2DINV Manual and Loke's Course Notes. A description of the different array types is given in the free tutorial notes on electrical imaging (Loke, 2004). The topography data are in the third section, below the section with the apparent resistivity values, separated by them by some specific flags. The first item is a flag that indicates whether the file
590 contains topography data. If there is no topography data, its value is 0. We entered 1 or 2 to indicate that topographical data was present. In most transects, the distances of the points are taken along the ground surface; in this case, the value of 2 for the topography data flag is considered. This is followed by the number of topographical data points. At the end, some 0 flags are included.

6.2.2 GPR files

595 The GPR data are available in SEG Y format (Hagelund and Levin, 2017) after being converted from the original files in proprietary RADAN format (with extension .DZT). The SEG Y is an open standard format developed by the Society of Exploration Geophysicists in 1975. Nevertheless, it remains the preferred preservation file format for GPR data. The files have been post-processed according to the workflow provided in Section 4 and then converted to SEG Y format. The conversion and post-processing were performed using Reflexw Software (Sandmeier, 2021). The conversion was performed
600 following these settings: exporting format SEG Y-DOS, scaling factor for coordinates equal to 1, and checking the output parameters "seg y_ibm_format" and "ps timeincr". This SEG Y format provides a file with IBM 32-bit floating-point numbers. We tested the files with Reflexw and GPR-Viewer to validate them before the publication.

7 Discussion

We presented a new set of geophysical data from the remote site of Ny-Ålesund in High Arctic environment. The multi-
605 method geophysical survey was designed to image the subsurface at different scales and resolutions. A thorough interpretation of all the 2D resistivity models goes beyond the scope of this paper, that was primarily conceived to share with the scientific community a large data set coming from a unique study area. In fact, a comprehensive interpretation would require an integrated approach, that is, further investigations on geology, geochemistry, and hydrogeological modelling because the study area is known to have complex heterogeneities in the subsurface and permafrost distribution (Orvin,
610 1934). Detailed analyses are ongoing as part of the I2F project and will consider the geophysical data set as a mosaic tile. To date, the published data set represents an invite to expand scientific knowledge of the Ny-Ålesund area by means of

geophysical proofs. Some food for thought is here proposed to stimulate future discussions and applications among the scientific community active in polar studies as well as in climate change studies.

7.1 Preliminary interpretation

615 A significant variability was observed in the measured ERT and GPR data, that is, in the apparent resistivity pseudosections for ERT and in GPR profiles. This implied various degrees of heterogeneity in the distribution of the imaged physical parameters, both electrical resistivity and dielectric permittivity. To explain this heterogeneity, several factors should be considered by the users and modelers of the data set. As is widely known, the electrical resistivity of the subsurface is usually controlled by lithology, the occurrence of liquid phase (that rules electrolytic conduction) and the amount of clay
620 (that enhances surface conduction). The peculiar conditions of the study area strongly affected the geophysical response. The occurrence of ice in the permafrost and intermittently in the active layer plays a relevant role in increasing the bulk resistivity of the subsurface. The data set can be modelled and interpreted in terms of percentage of ice content at depth, thus solving the challenge of a distinction between different solid and fluid phases involved in the system under investigation.

We showed the results from two different inspected sectors, i.e., the piezometer and the mine areas. The profiles
625 ERT_P1_Par (Fig. 6), GPR_P1_Par (Fig. 10) and GPR_long_40 (Fig. 11) are placed in the piezometer area, while profile ERT9 (Fig. 7) is placed in the mine area.

The results from ERT_P1_Par (Fig. 6) and GPR_P1_Par (Fig. 10) regarded the shallow subsurface (maximum depth of investigation 10 m) and revealed a clear change with depth of the correspondent physical parameters. From these results, it can be inferred that there is a clear discontinuity in resistivity at around 1.5-2 m b.g.l and a reflector at 50-55 ns. This may be
630 related to the interface between the active layer and the frozen ground. The physico-chemical parameters measured in the piezometers (P1-P4) during the week of the geophysical survey are useful for further considerations. These measurements consist of continuous data logs (every 15 minutes) of temperature, electrical conductivity and water level and then at specific days water was collected to measure temperature and electrical conductivity. In P1, which is located in the center of ERT_P1_Par, there was no detection of water during the geophysical survey and hence the water conductivity was not
635 measured. In P1, the day of the acquisition of ERT_P1_Par, the bottom-hole temperature was 1.3 °C, while the depth of the frozen level was 132 cm from ground surface one day before the ERT acquisition.

GPR_long_40 is placed in the piezometer area and the acquisition direction was from P1 to P4 towards the glacier Brøggerbreen (Fig. 2). As anticipated in Section 5.3, this profile crosses all the piezometers from P1 (at a distance of 120 m) to P4 (at a distance of 440 m). During the geophysical survey in summer 2022, P1 and P4 were dry, while P2 and P3 had
640 water inside. The water sampling performed the 23rd of July 2022 (four days before the ERT survey in the piezometer area) gave a water level of 95 and 77 cm b.g.l. for P2 and P3, respectively, and water conductivity of 665 and 682 µS/cm, respectively. Moreover, in the days of the ERT acquisitions around P2 and P3, the depth of the frozen level from ground surface was 123 cm in P2 and 200 cm in P3. The ERT data around P2 and P3 reflected in the pseudosections of apparent resistivity the possible presence of water. In fact, the apparent resistivity of the ERTs crossing P2 and P3 was lower than that

645 of ERTs crossing P1 and P4. These ERT data can be used to study groundwater or hydrogeological activity together with the geochemical analyses performed during the I2F project. The piezometer data are in good agreement not only with the ERT data acquired with 1 m of electrode spacing, but also with the GPR data acquired with the 400 MHz antenna. In fact, the radargrams close to P2 and P3 have discontinuous reflectors that can be explained by the presence of water, which attenuates the GPR signal, and by heterogenous properties of the frozen ground. In the whole study area, the interpretation of the geophysical data (and models) in terms of liquid phase within the ground should consider different origin, evolution, physico-chemical properties and hence different values of the electrical resistivity of the aqueous solutions.

As regards the deep resistive structures (up to 10000 Ωm) in the models of ERT_P1_Par (Fig. 6) and ERT9 (Fig. 7), there is a clear difference in their lateral extent even though the two models have different depths of investigation. While ERT_P1_Par presents a laterally homogeneous deep resistive region, ERT9, which is placed in the mine area, discloses a heterogeneous resistivity distribution that can be explained by complex hydrological dynamics or even by the traces of the past mining activity/tunnels, that are not mapped nor available. The lateral variability of the deep structures of the resistivity model of ERT9 was not surprising because it was already evident in the data, i.e., the apparent resistivity pseudosections of the mine area (see ERT4-9 in the repository) and also because there is evidence of heterogeneous permafrost since Orvin (1934). Moreover, given that Ny-Ålesund is a former coal mining town, the occurrence of various coal seams as well as the past anthropic activity should be considered as a possible source of electrical resistivity anomalies (Orvin, 1934). Decades of coal mining exploitation produced a dense network of tunnels, boreholes and pits in a number of mines. To the knowledge of the authors, information about the mine area is neither well organized in a systematic GIS database nor completely available in English language, except for a report of the mining activities in Orvin (1934). A dense and tangled mining tunnelling system which supposedly develops from the surface down to several tens of meters could play an important role in the distribution of electrical resistivity in the mine area at the foot of Mt. Zeppelin. ERT4 to ERT9 were acquired in the area of the ruins of the past exploited mines, where few abandoned entrances of the past tunnels could be recognized from surface because they are somehow preserved as the cultural heritage of Ny-Ålesund. Therefore, it may be inferred that the mine channels and abandoned empty or saturated tunnels affected the ERT data albeit their maps are not available.

The mine area hosts Ester Spring, that had a scarce water flux in July 2022 and almost no water in August 2022. The ERT profiles that cross Ester Spring are ERT5-7, where the apparent resistivity pseudosections clearly show an electrically conductive region below the spring.

7.2 Future work and other data in the area

The presented data set can be used for several scientific purposes. First, the ERT data can support studies on the interplay between groundwater and permafrost, thus improving knowledge about possible deep circulation of water supra, intra and sub-permafrost. Second, the integrated ERT and GPR data can offer the opportunity to identify both the interface between active layer and permafrost at very high latitudes and even the continuity of the permafrost in terms of ice percentage. The ERT data acquired with the maximum electrode spacing (10 m) provided the largest depth of investigation, i.e., around 100

m. The ERT data set is unlikely supposed to provide clear evidence of the bottom of the permafrost. Increasing the depth of investigation would be of uppermost scientific interest, given the deep heterogeneities that emerged from our data. To do that, future ERT surveys should consider a larger electrode spacing than 10 m or other geophysical techniques, such as time-domain EM. Future ERT surveys should pay particular attention to the contact resistance that may result high due to the gravelly or dry soil in proximity of the widespread moraine deposits.

Beyond the piezometer data, used in Section 7.1 for our preliminary interpretation and soon available as outcome of the I2F project (<https://www.icetoflux.eu/data>), other geological data have been identified in the area and can be used to further interpret our data set. General geological descriptions of our study area are available from Hoel (1925), Orvin (1934) and Horota et al. (2023). The appendix plates n. V, VI and VII in Orvin (1934) show some geological sections. Furthermore, several boreholes have been drilled in the surroundings, as shown in appendix plate n. III of Orvin (1934). Borehole n. 4 in Orvin (1934) was drilled in 1928 down to 149 m depth, ~100 m east from the end of our ERT1, according to our digitization from Orvin's plate n. III to WGS84-EPSS 4326 (78°55'12" N, 11°49'46" E). Borehole n. 2 from Orvin (1934) was drilled in 1928 down to 59 m depth to study a coal seam. It is located 67 m east from the end of our ERT10 and ~100 m south from our piezometer P4 (78°55'3" N, 11°51'8" E). Other three boreholes are reported in Orvin (1934), but they are ~500 m away from our ERT lines. Another borehole, called "Bayelva", was drilled 150 m south from the intersection of ERT1 and ERT2 (78°55'15" N, 11°50'03" E) by the Alfred Wegner Institute (AWI) in 2009 to monitor permafrost and active layer temperature down to 9.3 m depth (Boike et al., 2018; Orr et al., 2019). Unfortunately, the stratigraphic description is not reported. Last, around our piezometer area, a borehole called "DBNyÅlesund" (Orr et al., 2019) was drilled in 2015 by Insubria University down to 48.5 m depth at 78°55'14" N and 11°52'00" E, ~72 m north from the middle of our ERT3 and 208 m east of our piezometer P1. Yet the only information publicly available are the temperature time series and that its stratigraphy consists of 14 m of diamicton, possibly a glacial till, with bedrock below it (data accessible from: <https://sios-svalbard.org/node/648> and <http://gtnpdatabase.org/boreholes/view/1837/>). Future work could leverage these existing data and potentially conduct additional geological observations which, in combination with our data set, will allow a better description of the permafrost and hydrological regimes at our study sites.

8 Data availability

Data described in this manuscript can be accessed at the repository under data doi: <https://zenodo.org/doi/10.5281/zenodo.10260056> (Pace et al., 2023). The same geophysical data set can also be accessed from the I2F project website: <https://www.icetoflux.eu/products/>. The piezometer metadata can be accessed here: <https://www.icetoflux.eu/data/>.

9 Conclusions

This paper set out to share the data set of a geophysical survey, performed in the summer of 2022 in the Svalbard Archipelago, near the Ny-Ålesund settlement. The survey was undertaken to provide new insight into the hydrogeological characterization of the area.

We described the acquisition settings of ERT and GPR data in such an extreme environment, that of remote High Arctic tundra. The details of all the acquired profiles were listed. Then, the methods adopted for quality control and processing were illustrated. Some representative examples of processed data and inversion results were shown in this manuscript, and together with the whole data set, were organized to be shared in a public repository. All the transects are completed with the topographical information and have been tested by checking their integrity and functionality. The repository is available under data doi (Pace et al., 2023, <https://zenodo.org/doi/10.5281/zenodo.10260056>).

The public availability of this repository is of major relevance because to the authors' knowledge no data set of near-surface geophysical acquisitions, such as the one presented here, has been published, even though Ny-Ålesund represents the northernmost scientific hub in the High Arctic. The data were collected for 2D interpretation, but an attempt of pseudo-3D data processing could be possible, especially in the piezometer area. In this area, we also shared the data set of GPR data that could be useful for data integration or joint inversion. This would be a fruitful area for future work. Our data set could offer a good opportunity for geophysicists to develop new methodologies for interpreting geophysical data in the Arctic environment and for geoscientists, involved in studying the region, to corroborate their assumptions about the geological and hydrogeological settings of the area.

Future work will investigate the interpretation of the geophysical models by means of hydrogeological and geological information and in collaboration with other partners of the I2F project. The data set is shared with the scientific community for all the possible purposes. Future users are kindly asked to cite the present paper when using the data set.

Glossary

- DD: Dipole-Dipole Array configuration for ERT data
- ERT: Electrical Resistivity Tomography
- GPR: Ground Penetrating Radar
- GPS: Global Positioning System
- I2F: ICEtoFLUX project
- MT: Magnetotelluric method
- UTM: Universal Transverse Mercator
- WS: Wenner-Schlumberger Array configuration for ERT data
- WE: Wenner Array configuration for ERT data

Author contribution

Data curation: FP, AV, AG, GR, AS, LC;

740 data acquisition and fieldwork: FP, AV, AG, GR, AS, LC, IB;

methodology and modeling: FP, AV, AG, GR, AS, LC;

software: FP, AV, AG, GR, AS, LC;

supervision: AG, AS, MD;

visualization: FP, AV, GR, AS, LC;

745 writing – original draft: FP, AV, AG, GR, AS, LC;

writing – review & editing: all.

Competing interests

The authors declare that they have no conflict of interest.

Acknowledgements

750 The authors would like to thank Diego Franco (Politecnico di Torino) for his help in setting up the instrumentation before and after the Arctic expedition. Further thanks go to the station leaders of the Italian Arctic Station Marco Casula and Ombretta Dell'Acqua for their support during the fieldwork in summer 2022. The authors thank the editor and the reviewers for their valuable and helpful comments, that helped us improve the manuscript. We would also like to show our gratitude to the polar bears of the Svalbard Islands that did not eat us, this time.

755 Financial support

The research project ICEtoFLUX (“HydrologIcal changes in ArctiC Environments and water-driven biogeochemical FLUXes”) was financed by Arctic Research Program MUR, project number PRA 2021-0027, CUPB45F21001960001. The research activity of F. Pace was carried out within the Ministerial Decree no. 1062/2021 and received funding from the FSE REACT-EU - PON Ricerca e Innovazione 2014-2020.

760 References

Beka, T. I., Smirnov, M., Bergh, S. G., and Birkelund, Y.: The first magnetotelluric image of the lithospheric-scale geological architecture in central Svalbard, Arctic Norway, *Polar Research*, 34, 26766, <https://doi.org/10.3402/polar.v34.26766>, 2015.

- 765 Beka, T. I., Smirnov, M., Birkelund, Y., Senger, K., and Bergh, S. G.: Analysis and 3D inversion of magnetotelluric crooked profile data from central Svalbard for geothermal application, *Tectonophysics*, 686, 98–115, <https://doi.org/10.1016/j.tecto.2016.07.024>, 2016.
- Beka, T. I., Senger, K., Autio, U. A., Smirnov, M., and Birkelund, Y.: Integrated electromagnetic data investigation of a Mesozoic CO₂ storage target reservoir-cap-rock succession, Svalbard, *Journal of Applied Geophysics*, 136, 417–430, 770 <https://doi.org/10.1016/j.jappgeo.2016.11.021>, 2017a.
- Beka, T. I., Bergh, S. G., Smirnov, M., and Birkelund, Y.: Magnetotelluric signatures of the complex tertiary fold–thrust belt and extensional fault architecture beneath Brøggerhalvøya, Svalbard, *Polar Research*, 36, 1409586, <https://doi.org/10.1080/17518369.2017.1409586>, 2017b.
- Binley, A.: R2 (Version 4.10), 2023.
- 775 Blanchy, G., Saneiyani, S., Boyd, J., McLachlan, P., and Binley, A.: ResIPy, an intuitive open source software for complex geoelectrical inversion/modeling, *Computers & Geosciences*, 137, 104423, <https://doi.org/10.1016/j.cageo.2020.104423>, 2020.
- Boike, J., Juszak, I., Lange, S., Chadburn, S., Burke, E., Overduin, P. P., Roth, K., Ippisch, O., Bornemann, N., Stern, L., Gouttevin, I., Hauber, E., and Westermann, S.: A 20-year record (1998–2017) of permafrost, active layer and meteorological 780 conditions at a high Arctic permafrost research site (Bayelva, Spitsbergen), *Earth Syst. Sci. Data*, 10, 355–390, <https://doi.org/10.5194/essd-10-355-2018>, 2018.
- Booij, M., Leijnse, A., Haldorsen, S., Heim, M., and Rueslåtten, H.: Subpermafrost Groundwater Modelling in Ny-Ålesund, Svalbard, *Hydrology Research*, 29, 385–396, <https://doi.org/10.2166/nh.1998.0030>, 1998.
- Chave, A. D., Jones, A. G., Mackie, R., and Rodi, W.: *The Magnetotelluric Method: Theory and Practice*, Cambridge University Press, Cambridge, <https://doi.org/10.1017/CBO9781139020138>, 2012. 785
- Dallmann, W. K. (Ed.): *Geoscience atlas of Svalbard*, Norsk polarinstitutt, Tromsø, 292 pp., 2015.
- Doveri, M., Lelli, M., Baneschi, I., Raco, B., Trifirò, S., Calvi, E., and Provenzale, A.: Glacial drainages and transfer of freshwater to the Arctic Ocean in Kongsfjorden (Svalbard), 16518, 2019.
- Doyoro, Y. G., Chang, P.-Y., Puntu, J. M., Lin, D.-J., Van Huu, T., Rahmalia, D. A., and Shie, M.-S.: A review of open 790 software resources in python for electrical resistivity modelling, *Geosci. Lett.*, 9(1), 1–16, <https://doi.org/10.1186/s40562-022-00214-1>, 2022.
- Edwards, L. S.: A modified pseudosection for resistivity and IP, *GEOPHYSICS*, 42, 1020–1036, <https://doi.org/10.1190/1.1440762>, 1977.
- Geuzaine, C. and Remacle, J.-F.: Gmsh: A 3-D finite element mesh generator with built-in pre- and post-processing 795 facilities: THE GMSH PAPER, *Int. J. Numer. Meth. Engng.*, 79, 1309–1331, <https://doi.org/10.1002/nme.2579>, 2009.
- Gevers, M., David, D. T., Thakur, R. C., Hübner, C., and Jania, J.: *SESS report 2022*, Svalbard Integrated Arctic Earth Observing System, Longyearbyen, 2023.
- Hagelund, R. and Levin, S. A.: SEG-Y_r2.0: SEG-Y revision 2.0 Data Exchange format, SEG Technical Standards Committee, 1–151, <https://doi.org/10.1190/tle36050449.1>, 2017.

- 800 Haldorsen, S. and Heim, M.: An arctic groundwater system and its dependence upon climatic change: an example from Svalbard, *Permafrost and Periglacial Processes*, 10, 137–149, [https://doi.org/10.1002/\(SICI\)1099-1530\(199904/06\)10:2<137::AID-PPP316>3.0.CO;2-%23](https://doi.org/10.1002/(SICI)1099-1530(199904/06)10:2<137::AID-PPP316>3.0.CO;2-%23), 1999.
- Haldorsen, S., Heim, M., and Lauritzen, S.-E.: Subpermafrost Groundwater, Western Svalbard, *Hydrology Research*, 27, 57–68, <https://doi.org/10.2166/nh.1996.0019>, 1996.
- 805 Haldorsen, S., Heim, M., Lefauconnier, B., Pettersson, L.-E., Røros, M., and Sandsbråten, K.: The water balance of an arctic lake and its dependence on climate change: Tvillingvatnet in Ny-Ålesund, Svalbard, *Norsk Geografisk Tidsskrift - Norwegian Journal of Geography*, 56, 146–151, <https://doi.org/10.1080/002919502760056477>, 2002.
- Haldorsen, S., Heim, M., Dale, B., Landvik, J. Y., Van Der Ploeg, M., Leijnse, A., Salvigsen, O., Hagen, J. O., and Banks, D.: Sensitivity to long-term climate change of subpermafrost groundwater systems in Svalbard, *Quat. res.*, 73, 393–402, <https://doi.org/10.1016/j.yqres.2009.11.002>, 2010.
- 810 Haldorsen, S., Heim, M., and Van der Ploeg, M. J.: Impacts of climate change on groundwater in permafrost areas: case study from Svalbard, Norway, in: H. Treidel, J. L. Martin-Bordes, & J. J. Gurdak (Eds.), *Climate change effects on groundwater resources: a global synthesis of findings and recommendations*, IAH-International Contributions to Hydrogeology (pp. 323-338). (IAH - International Contributions to Hydrogeology)., 323–338, 2011.
- 815 Hansen, C. D. and Johnson, C. R. (Eds.): *The visualization handbook*, Elsevier-Butterworth Heinemann, Amsterdam ; Boston, 962 pp., 2005.
- Hauck, C. and Kneisel, C. (Eds.): *Applied Geophysics in Periglacial Environments*, 1st ed., Cambridge University Press, <https://doi.org/10.1017/CBO9780511535628>, 2008.
- Herring, T., Lewkowicz, A. G., Hauck, C., Hilbich, C., Mollaret, C., Oldenborger, G. A., Uhlemann, S., Farzamian, M., Calmels, F., and Scandroglio, R.: Best practices for using electrical resistivity tomography to investigate permafrost, *Permafrost & Periglacial*, 34, 494–512, <https://doi.org/10.1002/ppp.2207>, 2023.
- 820 Hill, G. J.: On the Use of Electromagnetics for Earth Imaging of the Polar Regions, *Surv Geophys*, 41, 5–45, <https://doi.org/10.1007/s10712-019-09570-8>, 2020.
- Hoel, A.: *The coal deposits and coal mining of Svalbard (Spitsbergen and Bear Island)*, Oslo, 92 pp., 1925.
- 825 Horota, R. K., Senger, K., Rodes, N., Betlem, P., Smyrak-Sikora, A., Jonassen, M. O., Kramer, D., and Braathen, A.: West Spitsbergen fold and thrust belt: A digital educational data package for teaching structural geology, *Journal of Structural Geology*, 167, 104781, <https://doi.org/10.1016/j.jsg.2022.104781>, 2023.
- Jol, H. M.: *Ground Penetrating Radar Theory and Applications*, Elsevier, <https://doi.org/10.1016/B978-0-444-53348-7.X0001-4>, 2009.
- 830 Kasprzak, M.: Seawater Intrusion on the Arctic Coast (Svalbard): The Concept of Onshore-Permafrost Wedge, *Geosciences*, 10, 349, <https://doi.org/10.3390/geosciences10090349>, 2020.
- Killingtveit, Å., Pettersson, L.-E., and Sand, K.: Water balance investigations in Svalbard, *Polar Research*, 22, 161–174, <https://doi.org/10.1111/j.1751-8369.2003.tb00105.x>, 2003.

- 835 Kodama, Y., Yukari, T., Hironori, N., and Okitsugu, W.: HYDROLOGICAL OBSERVATIONS IN BREGGER GLACIER BASIN, SPITSBERGEN : DISCHARGE, TEMPERATURE AND ELECTRIC CONDUCTIVITY, Proceedings of the NIPR Symposium on Polar Meteorology and Glaciology, 45–53, <https://doi.org/10.15094/00003878>, 1995.
- Koster, B. and Kruse, F.: The use of ground penetrating radar (GPR) in the investigation of historical quarry abandonment in Svalbard, *Polar Record*, 52, 330–344, <https://doi.org/10.1017/S0032247415000844>, 2016.
- 840 Kula, D., Olszewska, D., Dobiński, W., and Glazer, M.: Horizontal-to-vertical spectral ratio variability in the presence of permafrost, *Geophysical Journal International*, 214, 219–231, <https://doi.org/10.1093/gji/ggy118>, 2018.
- Kuschel, E., Eppinger, S., Bernard, E., Tolle, F., Prokop, A., Friedt, J.-M., and Zangerl, C.: Landslide monitoring using multi-temporal terrestrial laser scanning (TLS) and electrical resistivity tomography (ERT) in the high Arctic, Ny-Ålesund, *Geophysical Research Abstracts*, 21, 13733, 2019.
- 845 Lee, J.-S., Hong, W.-T., Park, K., Hong, S., Lee, S.-H., and Byun, Y.-H.: Evaluation of Water Content in an Active Layer Using Penetration-Type Time Domain Reflectometry, *Applied Sciences*, 8, 935, <https://doi.org/10.3390/app8060935>, 2018.
- Loke, M. H.: Tutorial: 2-D and 3-D electrical imaging surveys, 2004.
- Loke, M. H. and Barker, R. D.: Rapid least-squares inversion of apparent resistivity pseudosections by a quasi-Newton method1, *Geophys Prospect*, 44, 131–152, <https://doi.org/10.1111/j.1365-2478.1996.tb00142.x>, 1996.
- 850 Loke, M. H., Chambers, J. E., Rucker, D. F., Kuras, O., and Wilkinson, P. B.: Recent developments in the direct-current geoelectrical imaging method, *Journal of Applied Geophysics*, 95, 135–156, <https://doi.org/10.1016/j.jappgeo.2013.02.017>, 2013.
- Martorana, R., Capizzi, P., D’Alessandro, A., and Luzio, D.: Comparison of different sets of array configurations for multichannel 2D ERT acquisition, *Journal of Applied Geophysics*, 137, 34–48, <https://doi.org/10.1016/j.jappgeo.2016.12.012>, 2017.
- 855 Norwegian Polar Institute: Terrengmodell Svalbard (S0 Terrengmodell) [Data set]. Norwegian Polar Institute., <https://doi.org/10.21334/npolar.2014.dce53a47>, 2014.
- Oldenburg, D. W. and Li, Y.: Estimating depth of investigation in dc resistivity and IP surveys, *GEOPHYSICS*, 64, 403–416, <https://doi.org/10.1190/1.1444545>, 1999.
- 860 Orr, E., Hansen, G., Lappalainen, H., Hübner, C., and Lihavainen, H.: SESS report 2018, Svalbard Integrated Arctic Earth Observing System, Longyearbyen, 2019.
- Orvin, A. K.: Geology of the King’s Bay Region, Spitsbergen. By A. K. Orvin. *Skrifter om Svalbard og Ishavet* . Nr. 57. pp. 195, with 3 plates, 4 maps, and 52 text-figures. Oslo: Jacob Dybwad, 1934, *Geol. Mag.*, 57, 195, <https://doi.org/10.1017/S0016756800093328>, 1934.
- 865 Pace, F., Vergnano, A., Godio, A., Romano, G., Capozzoli, L., Baneschi, I., Doveri, M., and Santilano, A.: A new repository of electrical resistivity tomography and ground penetrating radar data from summer 2022 near Ny-Ålesund, Svalbard, Zenodo [data set] (0), <https://zenodo.org/doi/10.5281/zenodo.10260056>, 2023.
- Paglia, E.: A higher level of civilisation? The transformation of Ny-Ålesund from Arctic coalmining settlement in Svalbard to global environmental knowledge center at 79° North, *Polar Record*, 56, e15, <https://doi.org/10.1017/S0032247419000603>, 2020.

- 870 Pälli, A., Moore, J. C., Jania, J., Kolondra, L., and Glowacki, P.: The drainage pattern of Hansbreen and Werenskioldbreen, two polythermal glaciers in Svalbard, *Polar Research*, 22, 355–371, <https://doi.org/10.3402/polar.v22i2.6465>, 2003.
- Park, K., Kim, K., Kim, K., and Hong, W.-T.: Characterization of active layer at different degrees of patterned ground development using electrical resistivity tomography survey, *Cold Regions Science and Technology*, 208, 103734, <https://doi.org/10.1016/j.coldregions.2022.103734>, 2023.
- 875 Pedersen, Å. Ø., Convey, P., Newsham, K. K., Mosbacher, J. B., Fuglei, E., Ravolainen, V., Hansen, B. B., Jensen, T. C., Augusti, A., Biersma, E. M., Cooper, E. J., Coulson, S. J., Gabrielsen, G. W., Gallet, J. C., Karsten, U., Kristiansen, S. M., Svenning, M. M., Tveit, A. T., Uchida, M., Baneschi, I., Calizza, E., Cannone, N., De Goede, E. M., Doveri, M., Elster, J., Giamberini, M. S., Hayashi, K., Lang, S. I., Lee, Y. K., Nakatsubo, T., Pasquali, V., Paulsen, I. M. G., Pedersen, C., Peng, F., Provenzale, A., Pushkareva, E., Sandström, C. A. M., Sklet, V., Stach, A., Tojo, M., Tytgat, B., Tømmervik, H.,
880 Velazquez, D., Verleyen, E., Welker, J. M., Yao, Y.-F., and Loonen, M. J. J. E.: Five decades of terrestrial and freshwater research at Ny-Ålesund, Svalbard, *Polar Research*, 41, <https://doi.org/10.33265/polar.v41.6310>, 2022.
- Putkonen, J.: Soil thermal processes and heat transfer processes near Ny-Ålesund, northwestern Spitsbergen, Svalbard, *Polar Research*, 17, 165–179, <https://doi.org/10.3402/polar.v17i2.6617>, 1998.
- Repp, K.: The Hydrology of Bayelva, Spitsbergen, *Hydrology Research*, 19, 259–268, <https://doi.org/10.2166/nh.1988.0018>,
885 1988.
- Rønning, J. S.: Finetuning ground penetrating radar velocity analysis from hyperbola fitting using migration, *Near Surface Geophysics*, 21, 171–181, <https://doi.org/10.1002/nsg.12250>, 2023.
- Rossi, M., Dal Cin, M., Picotti, S., Gei, D., Isaev, V. S., Pogorelov, A. V., Gorshkov, E. I., Sergeev, D. O., Kotov, P. I., Giorgi, M., and Rainone, M. L.: Active Layer and Permafrost Investigations Using Geophysical and Geocryological
890 Methods—A Case Study of the Khanovey Area, Near Vorkuta, in the NE European Russian Arctic, *Front. Earth Sci.*, 10, 910078, <https://doi.org/10.3389/feart.2022.910078>, 2022.
- Sandmeier, K. J.: Reflexw Version 9.5 Windows™ XP/7/8/10-program for the processing of seismic, acoustic or electromagnetic reflection, refraction and transmission data, Sandmeyer geophysical research, 2021.
- Schwamborn, G., Heinzl, J., Schirrmeister, L., and Boike, J.: Verifying georadar records from permafrost in the Ny-
895 Ålesund area using core data and wavelet modelling, AWIPEV - Workshop, Joint French-German Collaborations for science in Svalbard, Strassbourg, France, 2005.
- Son, D. and Lee, E. J.: Soil Microbial Communities Associated with Three Arctic Plants in Different Local Environments in Ny-Ålesund, Svalbard, *J. Microbiol. Biotechnol.*, 32, 1275–1283, <https://doi.org/10.4014/jmb.2208.08009>, 2022.
- Svendsen, H., Beszczynska-Møller, A., Hagen, J. O., Lefauconnier, B., Tverberg, V., Gerland, S., Børre Ørbæk, J., Bischof, K., Papucci, C., Zajaczkowski, M., Azzolini, R., Bruland, O., and Wiencke, C.: The physical environment of Kongsfjorden–Krossfjorden, an Arctic fjord system in Svalbard, *Polar Research*, 21, 133–166, <https://doi.org/10.3402/polar.v21i1.6479>,
900 2002.
- Telford, W. M., Geldart, L. P., and Sheriff, R. E.: Applied geophysics, 2nd ed., Cambridge university press, Cambridge New York Port Chester [etc.], 1990.
- 905 Van der Ploeg, M. J.: Simulation of coupled groundwater flow and transport of heat in the groundwater system under Vestre Lovénbreen, with the model METROHEAT; a surveying study, 2002.

Wadhams, P.: A farewell to ice: a report from the Arctic, Oxford University Press, New York, NY, 2017.

910 Wannamaker, P., Hill, G., Stodt, J., Maris, V., Ogawa, Y., Selway, K., Boren, G., Bertrand, E., Uhlmann, D., Ayling, B.,
Green, A. M., and Feucht, D.: Uplift of the central transantarctic mountains, *Nat Commun*, 8, 1588,
<https://doi.org/10.1038/s41467-017-01577-2>, 2017.

Wannamaker, P. E., Stodt, J. A., and Olsen, S. L.: Dormant state of rifting below the Byrd Subglacial Basin, West
Antarctica, implied by magnetotelluric (MT) profiling, *Geophysical Research Letters*, 23, 2983–2986,
<https://doi.org/10.1029/96GL02887>, 1996.

915 Westermann, S., Wollschläger, U., and Boike, J.: Monitoring of active layer dynamics at a permafrost site on Svalbard using
multi-channel ground-penetrating radar, *The Cryosphere*, 4, 475–487, <https://doi.org/10.5194/tc-4-475-2010>, 2010.